Tailored Carbon Dioxide Capacity in Carboxylate-Based Ionic Liquids

Nicolas Scaglione, Jocasta Avila, Agilio Pádua, and Margarida Costa Gomes*

Laboratoire de Chimie de l'ENS Lyon, CNRS and Université de Lyon, 46 allée d'Italie, 69364 Lyon, France

E-mail: margarida.costa-gomes@ens-lyon.fr

Supplementary Information

Contents

1 Synthesis and Characterisation of the ILs

1.1 Ionic liquids synthesis

$[P_{4,4,4,4}][2-ClPyCOO]$, $[P_{4,4,4,4}][2-ClPhC_1OHCOO]$ and $[P_{4,4,4,4}][PhSC_1COO]$, whose structures are represented in Figure S1 were synthesized and characterized as described in our previous work.[1]

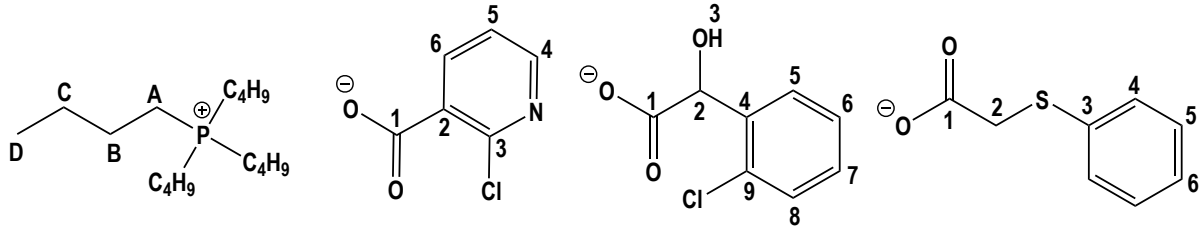

Figure S1 – Chemical structure of the newly prepared ILs: $[P_{4,4,4,4}][2-ClPyCOO]$, $[P_{4,4,4,4}][2-ClPhC_1OHCOO]$ and $[P_{4,4,4,4}][PhSC_1COO]$.

Tetrabutylphosphonium 2-chloropyridine-3-carboxylate $[P_{4,4,4,4}][2-ClPyCOO]$, the yellowish liquid obtained from the rotary evaporator was dried under vacuum (1×10^{-4} bar) at 323 K under stirring (400 rpm). The product was collected as a yellowish viscous liquid. ^{1}H NMR (400 MHz, C_6D_6, 343 K) δ ppm: 0.71 (t, 12H, $^3J_{HH} = 7.2$ Hz, D); 1.25 (m, 8H, C); 1.40 (m, 8H, B); 2.34 (m, 8H, A); 7.14 (t, 1H, $^3J_{HH}$= 4.9 Hz, 5); 7.63 (d, 1H, $^3J_{HH}$= 7.0 Hz, 6); 8.02 (m, 1H, 4). ^{13}C NMR (100 MHz, C_6D_6, 343 K) δ ppm: 12.43 (4C, D); 17.57 (4C, A); 22.70 (7C, B); 22.88 (4C, C); 121.54 (1C, 5); 136.33 (1C, 6); 139.71 (1C, 2); 145.60 (1C, 4); 146.43 (1C, 3); 166.01 (1C, 1). ^{31}P NMR (161 MHz, C_6D_6, 343 K) δ ppm: 33.66 (1P, $\mathbf{P}((CH_2)_3CH_3)_4$). ν (cm^{-1}): 2959; 2932; 2903; 2872; 1609; 1570; 1466; 1410; 1386; 1349; 1321; 1281; 1232; 1191; 1157; 1118; 1099; 1062; 1035; 1005; 969; 919; 909; 828; 812; 779; 752; 727; 643; 567; 554. MS ES^+ m/z (% Rel. Intensity): 259 (100, $[P_{4,4,4,4}]^+$). MS ES^- m/z (% Rel. Intensity): 156 (100, $[2-ClPyCOO]^-$).

Tetrabutylphosphonium 2-(2-chlorophenylacetate)-2-hydroxyacetate $[P_{4,4,4,4}][2-ClPhC_1OHCOO]$, the yellowish viscous liquid obtained from the rotary evaporator was dried under vacuum (1×10^{-4} bar) at 323 K under stirring (400 rpm). The product was collected as a dark yellowish viscous liquid.

^{1}H NMR (400 MHz, C_6D_6, 343 K) δ ppm: 0.71 (t, 12H, $^3J_{HH}$ = Hz, D); 1.20 (m, 14H, B+C); 2.04 (m, 8H, A); 4.79 (s, 1H, 2); 5.55 (s, 1H, 3); 6.95 (m, 2H, 7+8); 7.05 (m, 1H, 5); 7.24 (m,

1H, 6). ^{13}C NMR (100 MHz, C_6D_6, 343 K) δ ppm: 12.37 (4C, D); 17.33 (4C, A); 22.51 (4C, B); 22.80 (4C, C); 70.10 (1C, 2); 125.25 (1C, 7); 126.30 (1C, 8); 127.52 (1C, 6); 127.77 (1C, 5); 132.77 (1C, 4); 142.59 (1C, 9); 171.85 (1C, 1). ^{31}P NMR (161 MHz, C_6D_6, 343 K) δ ppm: 33.23 (1P, **P**$((CH_2)_3CH_3)_4$). ν (cm^{-1}): 3070; 2959; 2932; 2903; 2873; 1632; 1615; 1581; 1466; 1442; 1413; 1381; 1346; 1330; 1291; 1249; 1192; 1126; 1098; 1067; 1045; 1030; 1002; 969; 950; 925; 906; 871; 824; 782; 752; 722; 699; 609; 585; 570; 554. MS ES$^+$ m/z (% Rel. Intensity): 259 (100, $[P_{4,4,4,4}]^+$). MS ES$^-$ m/z (% Rel. Intensity): 185 (100, $[2-ClPhC_1OHCOO]^-$).

Tetrabutylphosphonium (thiophenyl)acetate [$P_{4,4,4,4}$][$PhSC_1COO$], the dark orange viscous liquid obtained from the rotary evaporator was dried under vacuum (1×10^{-4} bar) at 323 K under stirring (400 rpm). The product was collected as a orange-brown solid after drying under vacuum.

^{1}H NMR (400 MHz, C_6D_6, 343 K) δ ppm: ^{1}H NMR (400 MHz, C_6D_6, 343 K) δ ppm: 0.76 (t, 12H, $^3J_{HH} = 7.4$ Hz, D); 1.29 (m, 8H, C); 1.37 (m, 8H, B); 2.33 (m, 8H, A); 3.34 (s, 1H, 2); 6.87 (t, 1H, $^3J_{HH} = 7.4$ Hz, 6); 7.02 (m, 2H, $^3J_{HH} = 7.6$ Hz, 5); 7.14 (d, 2H, $^3J_{HH} = 7.8$ Hz, 4). ^{13}C NMR (100 MHz, C_6D_6, 343 K) δ ppm: 13.82 (4C, D); 18.87 (4C, A); 24.11, 24.29 (8C, B+C); 41.44 (1C, 2); 124.36 (1C, 6); 127.22 (2C, 4); 128.80 (2C, 5); 141.43 (1C, 3); 168.69 (1C, 1). ^{31}P NMR (161 MHz, C_6D_6, 343 K) δ ppm: 33.49 (1P, **P**$((CH_2)_3CH_3)_4$). ν (cm^{-1}): 2957; 2930; 2908; 2872; 1609; 1585; 1560; 1480; 1465; 1443; 1405; 1380; 1343; 1321; 1239; 1204; 1180; 1090; 1068; 1048; 1026; 1009; 968; 912; 907; 808; 737; 701; 691; 581; 575; 570; 561; 556. MS ES$^+$ m/z (% Rel. Intensity): 259 (100, $[P_{4,4,4,4}]^+$). MS ES$^-$ m/z (% Rel. Intensity): 167 (100, $[PhSC_1COO]^-$).

1.2 Density and molar volume

The experimental densities (ρ) and molar volumes (V_m) of the three new ILs are plotted in Figure S2 and listed in Table S1 along with the deviations of linear fits with temperature whose coefficients are listed in Tables S2 and S3, respectively. The presence of aromatic ring substituents in the carboxylate anions appears to result in denser ILs.

The V_m of these newly prepared ILs is additive and could be predicted using a group contribution method (GCM).[2] The calculated V_m agree with experimental values to within 2 % as

represented in Figure S2. The group contribution parameters are reported in Table S4.

Table S1 – Experimental densities and molar volumes of $[P_{4,4,4,4}][2-ClPyCOO]$, $[P_{4,4,4,4}][2-ClPhC_1OHCOO]$ and $[P_{4,4,4,4}][PhSC_1COO]$ in the temperature range of 293–363 K. The deviations (δ) reported are relative to the fitting polynomials with coefficients listed in Table S2 and Table S3.

$\frac{T}{K}$	$\frac{\rho}{g\,cm^{-3}}$	$\frac{\delta}{\%}$	$\frac{V_m}{cm^3\,mol^{-1}}$	$\frac{\delta}{\%}$	$\frac{T}{K}$	$\frac{\rho}{g\,cm^{-3}}$	$\frac{\delta}{\%}$	$\frac{V_m}{cm^3\,mol^{-1}}$	$\frac{\delta}{\%}$
	$[P_{4,4,4,4}][2-ClPyCOO]$					$[P_{4,4,4,4}][2-ClPhC_1OHCOO]$			
293.149	1.06170	0.003	391.81	0.02	293.151	1.06261	0.001	418.80	0.02
298.152	1.05860	0.005	392.96	0.00	298.150	1.05966	0.01	419.96	0.0005
303.151	1.05546	0.003	394.13	0.002	303.152	1.05653	0.005	421.21	0.004
313.152	1.04917	0.003	396.49	0.01	313.152	1.05030	0.004	423.71	0.008
323.152	1.04291	0.006	398.87	0.01	323.152	1.04412	0.008	426.21	0.01
333.152	1.03667	0.007	401.27	0.01	333.152	1.03799	0.008	428.73	0.01
343.152	1.03046	0.005	403.69	0.006	343.151	1.03188	0.005	431.27	0.005
353.152	1.02430	0.0006	406.12	0.003	353.152	1.02580	0.0003	433.83	0.004
363.152	1.01817	0.01	408.57	0.02	363.152	1.01977	0.01	436.39	0.01
	$[P_{4,4,4,4}][PhSC_1COO]$								
313.148	1.01071	0.007	422.12	0.006					
323.148	1.00451	0.001	424.72	0.002					
333.148	0.99834	0.006	427.35	0.004					
343.148	0.99223	0.006	429.98	0.004					
353.148	0.98616	0.001	432.63	0.001					
363.152	0.98012	0.007	435.29	0.006					

Table S2 – Fitting parameters A_0 and A_1 determined from the linear fitting of the experimental densities to $\rho = A_0 + A_1 T$ and the corresponding absolute average deviation (AAD).

Sample	$\frac{A_0}{g\,cm^{-3}}$	$\frac{A_1}{g\,cm^{-3}\,K}$	$\frac{AAD}{\%}$
$[P_{4,4,4,4}][2-ClPyCOO]$	1.2443	-6.2290 x 10^{-4}	0.004
$[P_{4,4,4,4}][2-ClPhC_1OHCOO]$	1.2425	-6.1377 x 10^{-4}	0.005
$[P_{4,4,4,4}][PhSC_1COO]$	1.2022	-6.1173 x 10^{-4}	0.004

Table S3 – Fitting parameters B_0 and B_1 determined from the linear fitting of the experimental molar volumes to $M_v = B_0 + B_1 T$ and the corresponding absolute average deviation (AAD).

Sample	$\frac{M}{g\,mol^{-1}}$	$\frac{B_0}{cm^3\,mol^{-1}}$	$\frac{B_1}{cm^3\,mol^{-1}\,K}$	$\frac{AAD}{\%}$
$[P_{4,4,4,4}][2-ClPyCOO]$	415.99	321.56	0.23940	0.009
$[P_{4,4,4,4}][2-ClPhC_1OHCOO]$	445.02	344.91	0.25174	0.009
$[P_{4,4,4,4}][PhSC_1COO]$	426.64	339.59	0.26340	0.004

Table S4 – Group contribution parameters used to calculate the molar volume of cation and anion as a function of temperature.

Group j	C_0 / $cm^3\ mol^{-1}$	C_1 / $cm^3\ mol^{-1}\ K$	C_2 / $cm^3\ mol^{-1}\ K^2$	Ref.
$-CH_2$	16.967	1.399 x 10^{-3}	-1.946 x 10^{-6}	2
$-CH_2-Ph$	80.185	1.344 x 10^{-1}	1.230 x 10^{-4}	2⋆
$-OH$	10.624	-3.319 x 10^{-2}	-4.034 x 10^{-5}	2⋆
$-Cl$	26.830	-7.000 x 10^{-4}	-4.250 x 10^{-5}	2
$-S-$	23.361	-1.814 x 10^{-1}	2.770 x 10^{-3}	3† ⋆
$-ClPy$	78.449	7.872 x 10^{-2}	4.3316 x 10^{-4}	2⋆
$-COO^-$	21.680	3.101 x 10^{-2}	-4.333 x 10^{-4}	4
$-CH_3COO^-$	49.177	2.149 x 10^{-2}	-2.775 x 10^{-5}	2
$[P_{4,4,4,4}]^+$	290.987	3.192 x 10^{-1}	1.436 x 10^{-5}	2⋆

⋆ Calculated by subtraction of parameters available in the reference.

† Calculated from the density data from the reference with temperatures ranging from 283 to 343 K.

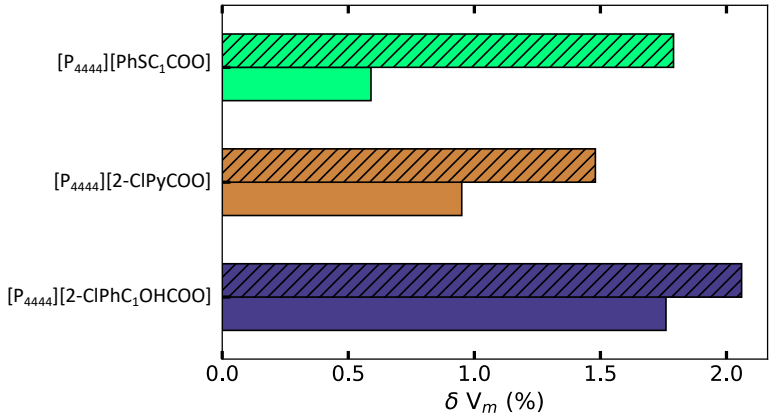

Figure S2 – Deviation of the predicted molar volumes[2] (V_m pred.) from the experimental values (V_m exp.) at 333 K (plain bars) and 353 K (textured bars).

1.3 Viscosity

The measured viscosity of the newly prepared ILs are listed in Table S5.

The experimental viscosities were fitted with temperature by using the Vogel-Fulcher-Tammann (VTF) equation:

$$\eta = A \exp\left(\frac{B}{T - T_0}\right) \tag{S1}$$

where η is the dynamic viscosity, T the temperature, and A, B, and T_0 are adjustable parameters. Their values for the ILs newly prepared are provided in Table S6. The experimental data are well repre-

sented by the fits with absolute average deviations (AAD) of up to 2.7 %.

Table S5 – Experimental viscosities of $[P_{4,4,4,4}][PhSC_1COO]$, $[P_{4,4,4,4}][2-ClPyCOO]$ and $[P_{4,4,4,4}][2-ClPhC_1OHCOO]$ in the temperature range of 303–363 K. The deviations (δ) reported are relative to the fitting of the VFT function with coefficients listed in Table S6.

T/K	η/mPa s	δ/%	T/K	η/mPa s	δ/%	T/K	η/mPa s	δ/%
$[P_{4,4,4,4}][2-ClPyCOO]$			$[P_{4,4,4,4}][2-ClPhC_1OHCOO]$			$[P_{4,4,4,4}][PhSC_1COO]$		
303.15	1222	0.07						
313.15	533.4	1.1	313.15	752.5	0.01			
323.15	282.0	3.11	323.15	377.2	0.1	323.15	119.1	0.005
333.15	156.3	1.6	333.15	205.8	0.2	333.15	72.90	0.03
343.15	89.20	5.4	343.15	121.2	0.3	343.15	47.49	0.04
353.15	59.54	3.1	353.15	76.06	0.03	353.15	32.60	0.08
363.15	40.52	4.4	363.15	50.73	1.2	363.15	23.42	0.1

Table S6 – Fitting parameters A, B and T_0 determined from the fitting of the experimental viscosities to the VFT function and the corresponding absolute average deviation (AAD).

Sample	A/mPa s	B/K	T_0/K	AAD/%
$[P_{4,4,4,4}][2-ClPyCOO]$	0.1635	884.18	204.01	2.7
$[P_{4,4,4,4}][2-ClPhC_1OHCOO]$	0.0346	1341.83	178.81	0.31
$[P_{4,4,4,4}][PhSC_1COO]$	0.0973	958.06	188.41	0.06

1.4 Thermal analysis

The melting points (T_{fus}) and phase-transition temperatures (T_{trans}) of the three newly synthesized ILs are listed in Table S7, and the corresponding thermograms are depicted in Figure S3. A meting point was only detected for $[P_{4,4,4,4}][PhSC_1COO]$ at $T_{fus} = 57.4$ °C and a solid-solid transition at $T_{trans} = 48.9$ °C. The melting point of $[P_{4,4,4,4}][PhSC_1COO]$ was verified using a melting point apparatus, providing an observable verification. For $[P_{4,4,4,4}][2-ClPyCOO]$ and $[P_{4,4,4,4}][2-ClPhC_1OHCOO]$, glass transition temperatures (T_g) were observed at −45.9 °C and −44.0 °C, respectively. $[P_{4,4,4,4}][PhSC_1COO]$ also exhibits a glass transition, but at a lower temperature of −53.0 °C.

Table S7 – Glass transition temperatures (T_g), melting points (T_{fus}) and crystallization temperatures (T_{cr}) for $[P_{4,4,4,4}][PhSC_1COO]$, $[P_{4,4,4,4}][2-ClPyCOO]$ and $[P_{4,4,4,4}][2-ClPhC_1OHCOO]$ measured in a DSC with a 10 K min^{-1} heating or cooling rate.

Sample	T_g / °C	T_{trans} & T_{fus} / °C	T_{cr} / °C
$[P_{4,4,4,4}][2-ClPyCOO]$	-45.9	-	-
$[P_{4,4,4,4}][2-ClPhC_1OHCOO]$	-44.0	-	-
$[P_{4,4,4,4}][PhSC_1COO]$	-53.4	46.1 & 57.6	-19.1

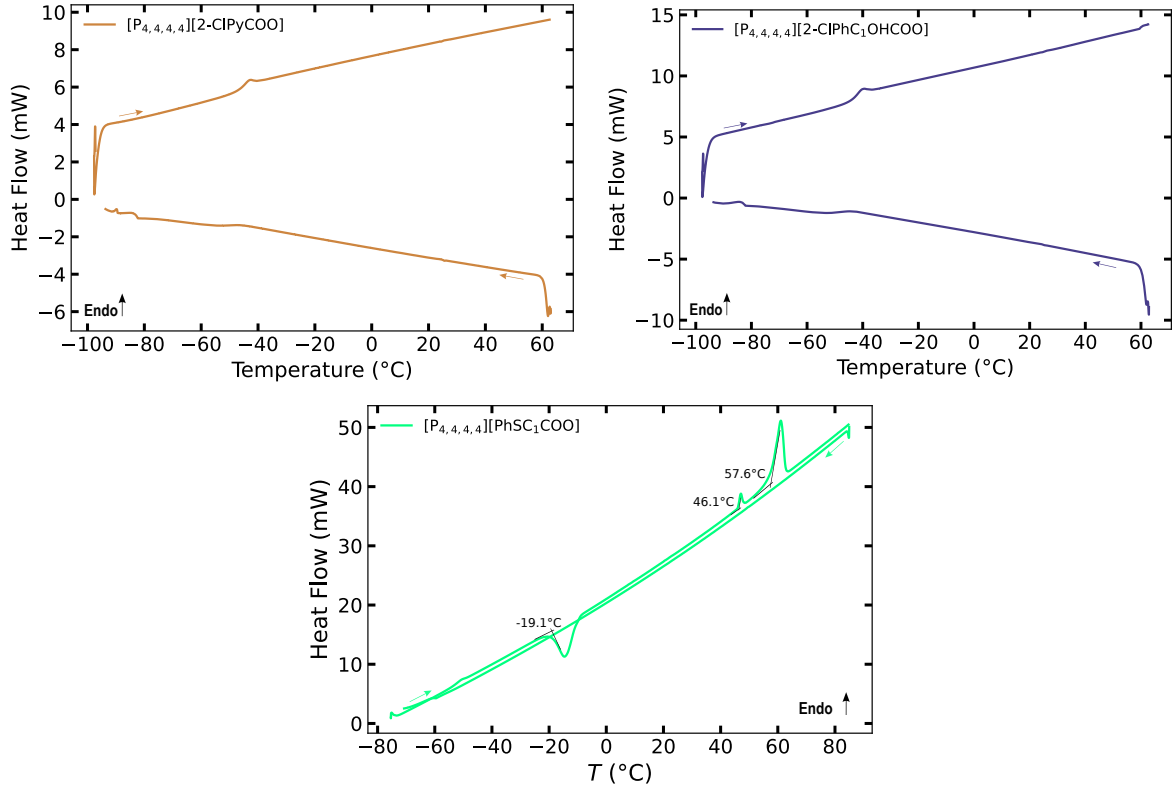

Figure S3 – Thermograms of — $[P_{4,4,4,4}][2-ClPyCOO]$, — $[P_{4,4,4,4}][2-ClPhC_1OHCOO]$ and — $[P_{4,4,4,4}][PhSC_1COO]$ measured at 10 K min^{-1}.

The thermal stability of the three newly synthesized ILs was investigated under an O_2 atmosphere, as the presence of O_2 can potentially affect IL stability due to its oxidizing properties. The decomposition temperatures (T_{dec}) of the ILs are listed in Table 1, and their corresponding thermographs are shown in Figure S4. Both $[P_{4,4,4,4}][2-ClPyCOO]$ and $[P_{4,4,4,4}][2-ClPhC_1OHCOO]$ exhibited a similar T_{dec} (261 °C), indicating comparable thermal stability. On the other hand, the T_{dec} of $[P_{4,4,4,4}][PhSC_1COO]$ was slightly higher at (276 °C). Their decomposition temperatures are close to those of other ILs containing carboxylate anions containing aromatic moieties.[1]

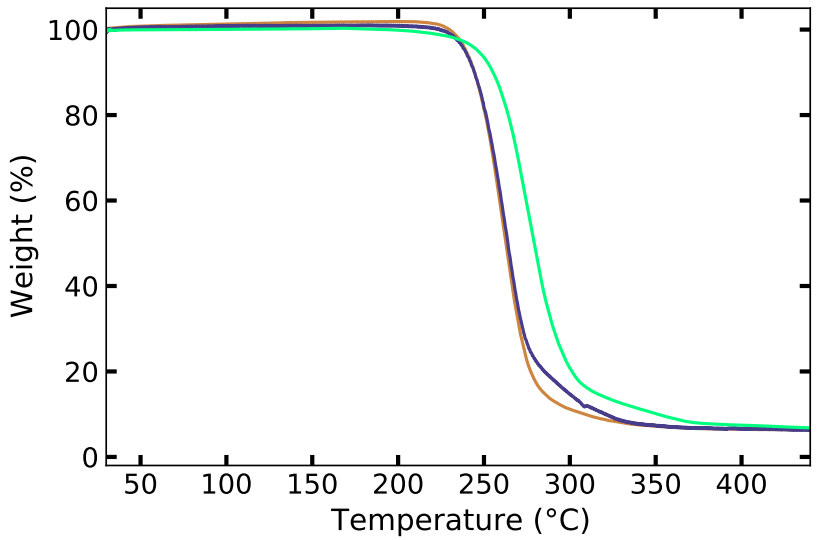

Figure S4 – TGA thermographs of — $[P_{4,4,4,4}][2-ClPyCOO]$, — $[P_{4,4,4,4}][2-ClPhC_1OHCOO]$ and — $[P_{4,4,4,4}][PhSC_1COO]$ with a heat rate of 10 °C min^{-1} under O_2. The decomposition temperatures were determined by the intersection of the tangents to the lines at low temperature and those corresponding to the rapid mass loss.

A considerable decrease in temperature was found from T_{dec} (254–345 °C) to $T_{0.01/10}$ (103–157 °C), confirming the overestimation of temperature-ramped TGA measurements. The long-term stability order of the ILs is also different and increases as follows: $[C_1COO]^- < [MeC_3COO]^- < [Me_4C_4COO]^- < [C_5COO]^- < [C_{11}COO]^- < [c-C_6COO]^- < [PhSC_1COO]^- < [PhC_1COO]^- < [TetrazC_1COO]^- < [2-ClPyCOO]^- < [2-ClPhC_1OHCOO]^-$ with $[P_{4,4,4,4}]^+$ as common cation. When aromatic moieties are part of the carboxylate anions, higher $T_{0.01/10}$ values were found while their T_{dec} values are significantly lower. These results highlight the importance of studying both long-term and short-term thermal stability when designing ILs for a given application. Interestingly enough, some trends remain consistent, such as the increased stability with the elongation of alkyl chain length in either the carboxylate anion or the phosphonium cation.

The pre-exponential factor A of the ILs containing $[P_{4,4,4,4}]^+$ as cation increases following a different trend: $[C_{11}COO]^- < [PhSC_1COO]^- < [C_1COO]^- \approx [c-C_6COO]^- \approx [C_5COO]^- < [MeC_3COO]^- < [Me_4C_4COO]^- < [TetrazC_1COO]^- < [PhC_1COO]^- < [2-ClPhC_1OHCOO]^- < [2-ClPyCOO]^-$, with a difference of nearly 14 orders of magnitude between the two extremes. It indicates that the structure of the carboxylate anion substituent significantly influences the value of the pre-exponential factor A, with higher values corresponding to more mobile ions. However, the size of the cation does not play a decisive role, as $[P_{6,6,6,14}][C_{11}COO]$ exhibits a higher A value than $[P_{4,4,4,4}][C_{11}COO]$, while the reverse trend is observed for $[P_{6,6,6,14}][Me_4C_4COO]$ and $[P_{4,4,4,4}][Me_4C_4COO]$. Despite the superior long-term

thermal stability of ILs compared to $[C_2C_1im][C_1COO]$ and $[C_2C_1C_1im][C_1COO]$, their activation energy (E_a) values were either lower or within a similar range, with the exception of $[P_{4,4,4,4}][PhC_1COO]$, $[P_{4,4,4,4}][2-ClPyCOO]$, and $[P_{4,4,4,4}][2-ClPhC_1OHCOO]$, which exhibited significantly higher E_a.

Table S8 – Long-term decomposition temperatures ($T_{0.01/10}$), the activation energy (E_a) and pre-exponential factor (A) determined for all the ILs under study following the MacFarlane method[5] under an atmosphere of O_2.

Sample	$T_{0.01/10}$ / °C	E_a / kJ mol^{-1}	A
$[P_{4,4,4,4}][2-ClPyCOO]$	156.8	194.56	1.27×10^{19}
$[P_{4,4,4,4}][TetrazC_1COO]$[6]	132.5	115.00	2.03×10^{10}
$[P_{4,4,4,4}][2-ClPhC_1OHCOO]$	145.4	153.30	4.26×10^{14}
$[P_{4,4,4,4}][C_1COO]$	102.9	92.86	1.23×10^{8}
$[P_{4,4,4,4}][PhSC_1COO]$	122.9	83.83	2.72×10^{6}
$[P_{4,4,4,4}][PhC_1COO]$	124.0	143.38	1.21×10^{14}
$[P_{4,4,4,4}][C_1COO]$	102.9	92.86	1.23×10^{8}
$[P_{4,4,4,4}][MeC_3COO]$	108.8	97.88	5.30×10^{8}
$[P_{4,4,4,4}][c-C_6COO]$	118.0	95.22	1.26×10^{8}
$[P_{4,4,4,4}][C_5COO]$	112.3	93.51	1.31×10^{8}
$[P_{4,4,4,4}][C_{11}COO]$	114.1	85.06	6.25×10^{5}
$[P_{6,6,6,14}][C_{11}COO]$	123.0	93.77	7.92×10^{7}
$[P_{4,4,4,4}][Me_4C_4COO]$	110.7	105.06	6.34×10^{9}
$[P_{6,6,6,14}][Me_4C_4COO]$	124.9	95.59	1.28×10^{8}

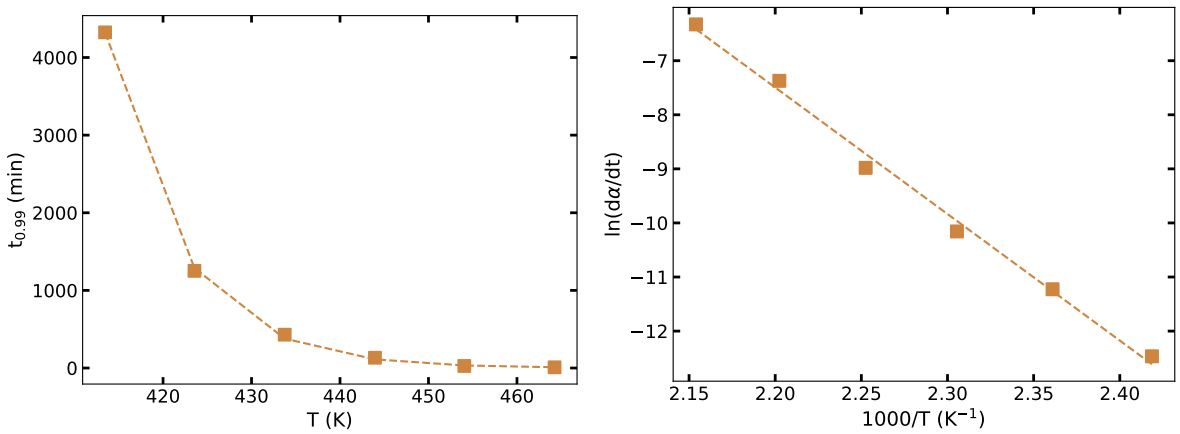

Figure S5 – Typical plot of (left) $t_{0.99}$, which is the time required to observe a decomposition of 1 % of the sample mass, as a function of temperature and (right) of $\ln(\frac{d\alpha}{dt})$ as a function of $1000/T$ for ■ $[P_{4,4,4,4}][2-ClPyCOO]$. Similar behaviours are found for the other ILs studied. Points are experimental and dashed lines are fitted curves.

1.5 Force field

Table S9 – Calculated densities of $[P_{4,4,4,4}][PhSC_1COO]$, $[P_{4,4,4,4}][2-ClPyCOO]$ and $[P_{4,4,4,4}][2-ClPhC_1OHCOO]$ with the new CL&Pol polarizable force field parameters[7] at different temperatures with the deviations from experimental densities.

Sample	$\frac{T}{K}$	$\frac{\rho_{exp}}{g\,cm^{-3}}$	$\frac{\rho_{calc}}{g\,cm^{-3}}$	$\frac{\delta}{\%}$
$[P_{4,4,4,4}][2-ClPyCOO]$	303	1.05546	1.04927	-0.59
	343	1.03047	1.02150	-0.87
$[P_{4,4,4,4}][2-ClPhC_1OHCOO]$	303	1.05653	1.05777	0.11
	343	1.03188	1.02356	-0.81
$[P_{4,4,4,4}][PhSC_1COO]$	343	0.99223	0.98264	-0.97

The force field was also employed to determine the self-diffusion coefficients of the ILs by fitting the mean squared displacements (MSD) obtained from the MD trajectories. The MSD analysis was performed after reaching the diffusive regime, typically observed between 3 and 18 ns. The calculated coefficients were found to be slightly underestimated compared to the experimental values (Table S14), with differences typically ranging from 20–30 % (Table S10). Similar self-diffusion coefficients for both cations and anions were also calculated for all the ILs confirming this feature. Furthermore, the more viscous ILs exhibited lower self-diffusion coefficients compared to their less viscous counterparts.

Table S10 – Simulated self-diffusion coefficients of $[P_{4,4,4,4}][2-ClPyCOO]$, $[P_{4,4,4,4}][2-ClPhC_1OHCOO]$ and $[P_{4,4,4,4}][PhSC_1COO]$ at 343 K by fitting the MSD calculated from MD simulations.

Sample (simulated)	$\frac{T}{K}$	$\frac{D_{anion}}{m^2\,s^{-1}}$	$\frac{D_{cation}}{m^2\,s^{-1}}$
$[P_{4,4,4,4}][2-ClPyCOO]$	343	1.05 ± 0.003	0.99 ± 0.002
$[P_{4,4,4,4}][2-ClPhC_1OHCOO]$	343	0.84 ± 0.002	0.85 ± 0.003
$[P_{4,4,4,4}][PhSC_1COO]$	343	0.96 ± 0.003	1.00 ± 0.002

1.6 Microscopic structure of the ILs

Appropriate radial or spatial distribution functions (RDFs and SDFs, respectively) were calculated for the three ILs synthesized herein. The RDFs of the P^+ and H_α sites of the $[P_{4,4,4,4}]^+$ cation around the carboxylate head group O_{COO^-} of the anions in $[P_{4,4,4,4}][PhSC_1COO]$, $[P_{4,4,4,4}][2-ClPyCOO]$, and $[P_{4,4,4,4}][2-ClPhC_1OHCOO]$ are shown in Figure S6 and compared with $[P_{4,4,4,4}][PhC_1COO]$ as a representative example of the carxoxylate ILs previously studied.[1]

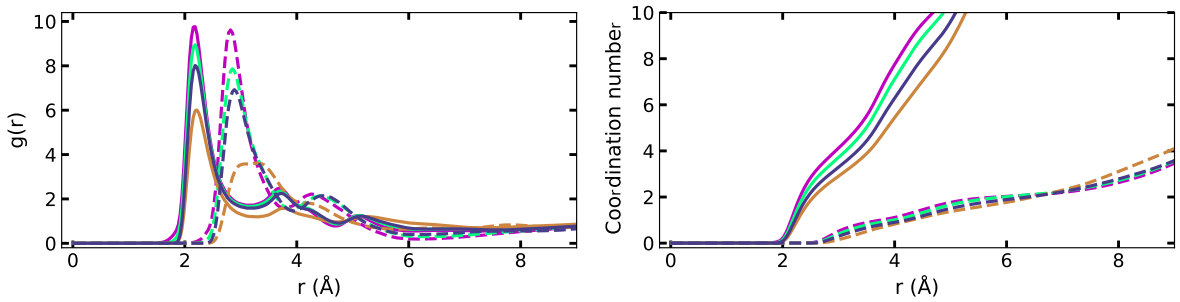

Figure S6 – Comparison of the site-site RDFs, $g_{ij}(r)$, of (dashed lines) P^+ and (solid lines) H_α of the cation around the negatively charged oxygen atoms O_{COO^-} of the carboxylate head of the anion and their corresponding coordination numbers in — $[P_{4,4,4,4}][PhC_1COO]$, — $[P_{4,4,4,4}][2-ClPyCOO]$, — $[P_{4,4,4,4}][2-ClPhC_1OHCOO]$ and — $[P_{4,4,4,4}][PhSC_1COO]$ at 343 K. The RDFs of $[P_{4,4,4,4}][PhC_1COO]$ were used as a representative example of the other ILs previously studied.[1]

Only $[P_{4,4,4,4}][2-ClPyCOO]$ exhibits slightly different RDFs between P^+ and H_α and O_{COO^-}, indicating a less significant correlation between these sites. This is further supported by the lower calculated coordination numbers (CNs) from approximately 1 and 4.5 to 0.79 and 3.35, respectively. Figure S7 (left) demonstrates that these reduced correlations arise from the presence of new correlations between the N of the carboxylate anion and P^+ and H_α of the phosphonium cation, as well as between Cl and H_α as illustrated on the SDF Figure S8. In $[P_{4,4,4,4}][2-ClPhC_1OHCOO]$, Figure S7 (right) reveals a low correlation between the O_{OH} of the carboxylate anion and H_α although it is not important enough to significantly affect the main interacting sites. These MD simulations provide valuable insights into the structural properties of the investigated ILs and offer a deeper understanding of their intermolecular interactions.

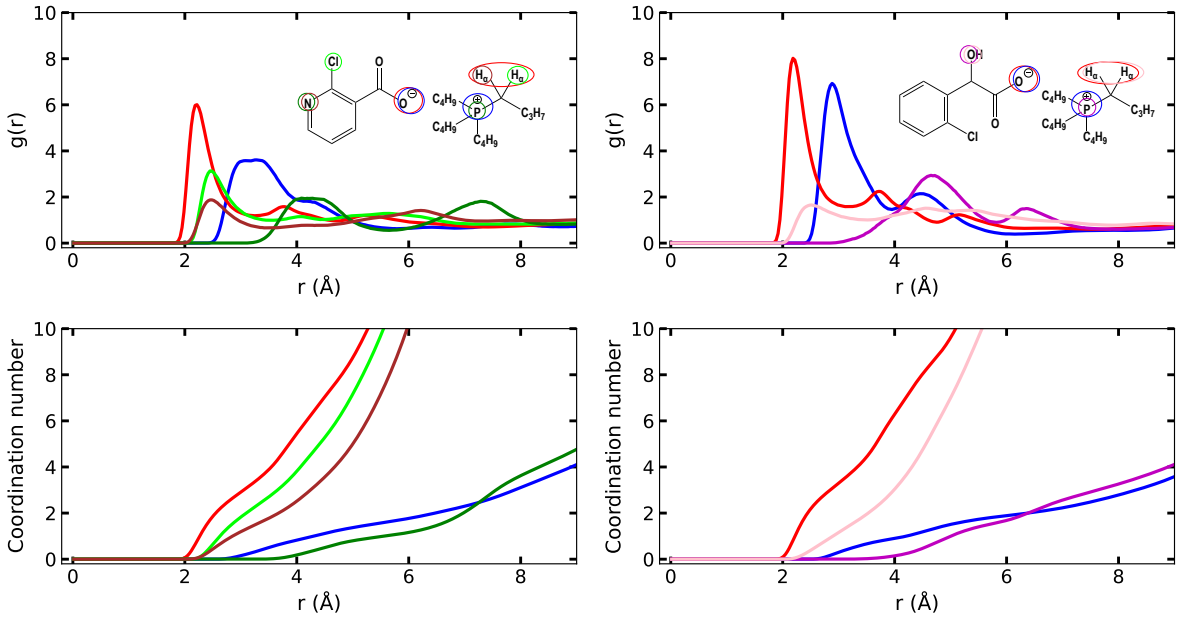

Figure S7 – Site-site RDFs, $g_{ij}(r)$, of — P^+ and — H_α of the cation around O_{COO^-} of the carboxylate anion and (left) H_α around — Cl and — N, — P^+ around N in $[P_{4,4,4,4}][2-ClPyCOO]$; (right) — P^+ and — H_α of the cation around O_{OH} in $[P_{4,4,4,4}][2-ClPhC_1OHCOO]$ at 343 K.

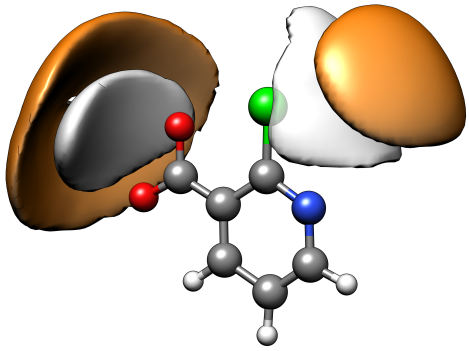

Figure S8 – The spatial distribution functions (SDFs) of P^+ (in orange) and of the acidic protons H_α (in white) around the O_{COO^-} of the $[2-ClPyCOO]^-$ anion in $[P_{4,4,4,4}][2-ClPyCOO]$ at 343 K. Isodensity contours at 14.7 and 7.9 times the average density around the central anion, respectively.

The combined distribution functions (CDFs) of the $C_\alpha-H_\alpha\cdots O_{COO^-}$ angle as a function of the distance between the acidic proton H_α and O_{COO^-} have also been calculated at 343 K (Figure S9). The CDFs reveal that not only the distance between the acidic proton and the carboxylate head are similar, but also the angles between them are identical at around 120 ° in these 3 new ILs. These angles are too low to be considered as proper hydrogen bonds.

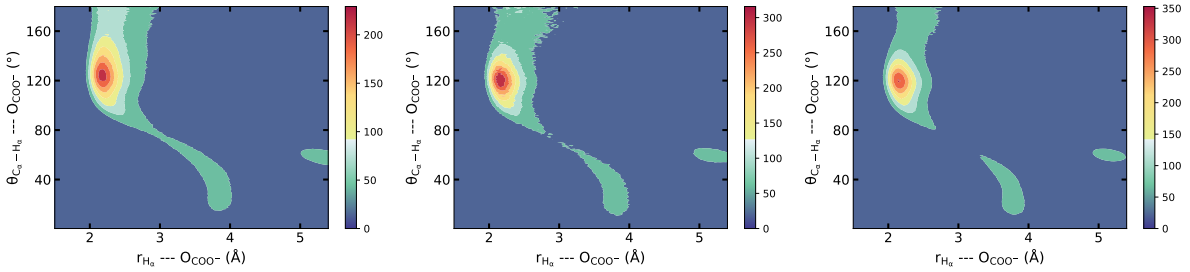

Figure S9 – Combined distribution functions (CDFs) of the $C_\alpha{-}H_\alpha\cdots O_{COO^-}$ angle as a function of the distance between the acidic proton H_α and the negatively charged O_{COO^-} in (left) $[P_{4,4,4,4}][2\ {-}ClPyCOO]$, (middle) $[P_{4,4,4,4}][2\ {-}ClPhC_1OHCOO]$ and (right) $[P_{4,4,4,4}][PhSC_1COO]$ at 343 K.

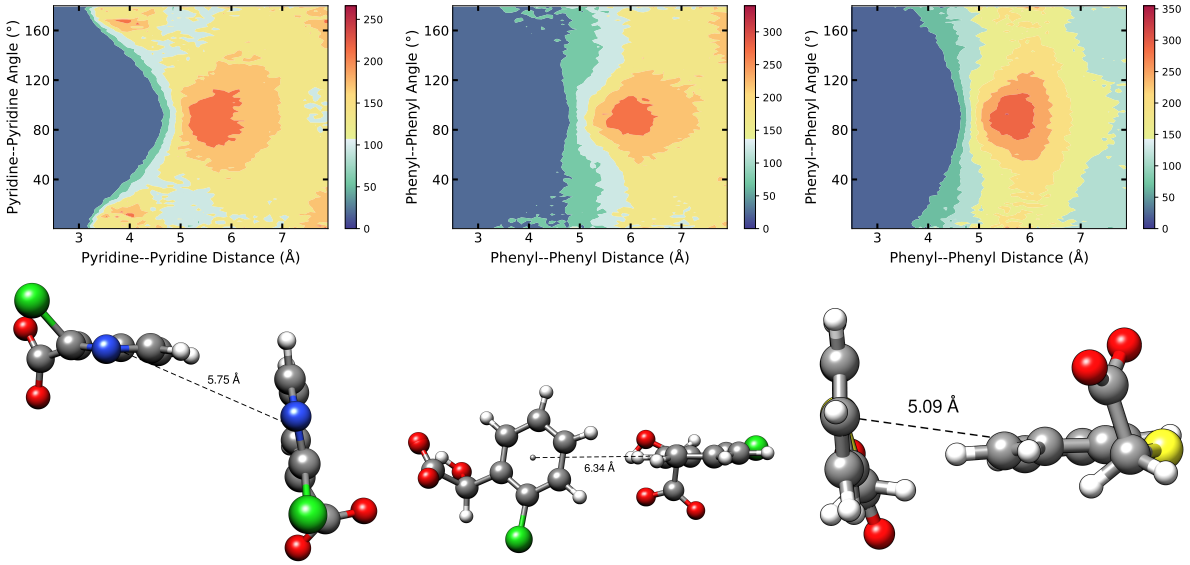

Figure S10 – CDFs of the angle between (left) two adjacent pyrridine rings in $[P_{4,4,4,4}][2\ {-}ClPyCOO]$, two adjacent phenyl rings (middle) in $[P_{4,4,4,4}][2\ {-}ClPhC_1OHCOO]$ and (right) in $[P_{4,4,4,4}][PhSC_1COO]$ as a function of the RDF between their center of mass at 343 K. (Bottom) Snapshots from the molecular simulation box showing the most probable spatial configuration of two neighbour anions.

$[P_{4,4,4,4}][PhSC_1COO]$, $[P_{4,4,4,4}][2\ {-}ClPyCOO]$ and $[P_{4,4,4,4}][2\ {-}ClPhC_1OHCOO]$ are presenting peculiar spatial configurations that can be attributed to the presence of aromatic moieties in the carboxylate anions. While one could expect a π-π stacking, the aromatic rings of the carboxylate anions are perpendicular to each other at a distance of 5.09, 5.75 and 6.34 Å, respectively. It is showed on the CDFs of the angle between two adjacent aromatic rings as a function of the RDF between their center of mass and illustrated by the snapshot from their molecular simulation box (Figure S10). This particular spatial configuration has also been found previously in the other ILs containing aromatic or aliphatic rings in the carboxylate anions.[1]

1.7 Small angle X-ray scattering

The experimental total structure factors of the three synthesised ILs are represented in Figure S11. The positions of the pre-peak, the shoulder and the principal peak are reported in Table S11. The total $S(q)$ calculated by MD simulations agree with the experimental data and so the calculated partial structure factors can be used to get further insights about the structure of the ILs. No particular features could be identified in the three ILs prepared herein when compared with the ones previously characterized.[1]

Table S11 – SAXS diffraction peak positions, q, their corresponding real space length, d, and the ion pair diameter, D, of $[P_{4,4,4,4}][2-ClPyCOO]$, $[P_{4,4,4,4}][2-ClPhC_1OHCOO]$ and $[P_{4,4,4,4}][PhSC_1COO]$. D was estimated by taking the cubic root of the volume of a single ion pair of the IL which was calculated from its molar volume and by assuming a cubic packing geometry.[8]

Sample	Pre-peak		Shoulder peak		Principal peak		
	q / Å^{-1}	d / Å	q / Å^{-1}	d / Å	q / Å^{-1}	d / Å	D / Å
$[P_{4,4,4,4}][2-ClPyCOO]$	0.57	11.0	0.72	8.7	1.38	4.6	8.7
$[P_{4,4,4,4}][2-ClPhC_1OHCOO]$	0.59	10.6	0.67	9.4	1.38	4.6	8.9
$[P_{4,4,4,4}][PhSC_1COO]$	0.58	10.8	-	-	1.46	4.3	8.9

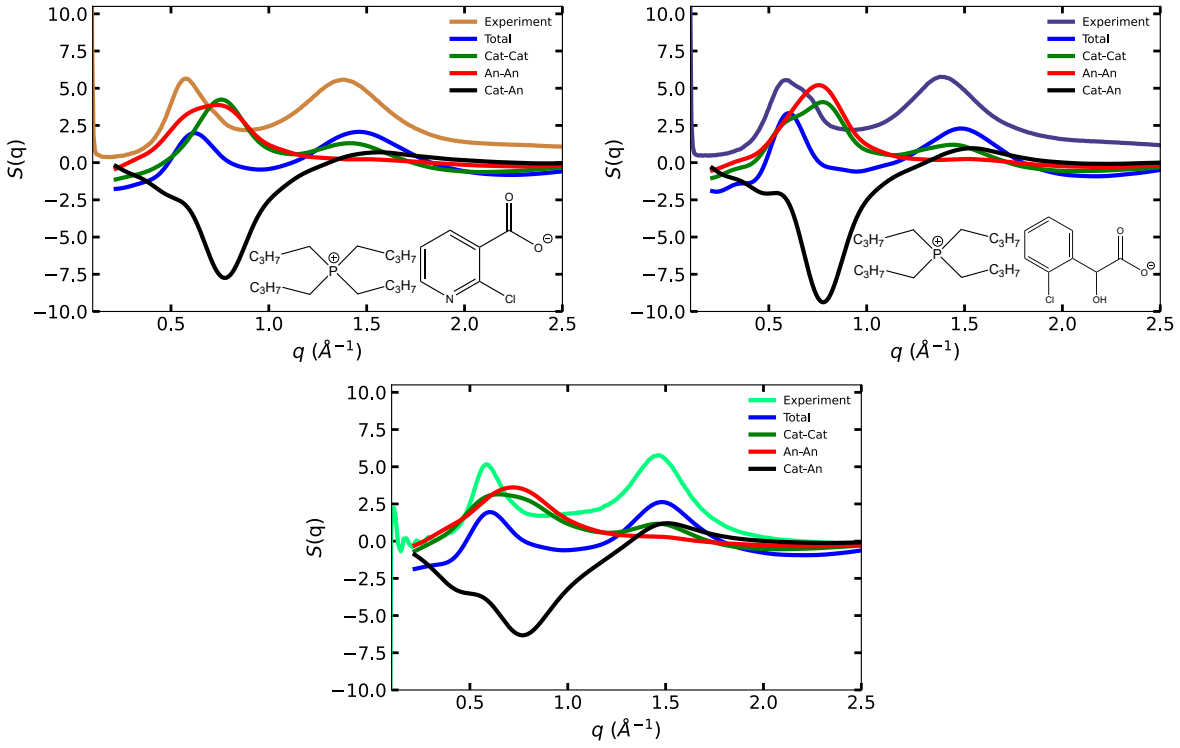

Figure S11 – Comparison of experimental with the total simulated $S(q)$ as well as the partial $S(q)$ for (top left) $[P_{4,4,4,4}][2-ClPyCOO]$, (top right) $[P_{4,4,4,4}][2-ClPhC_1OHCOO]$ and (bottom) $[P_{4,4,4,4}][PhSC_1COO]$.

2 Gas absorption data

Table S12 – Absorption and desorption of CO_2 in the ILs as a function of pressure from 0–5 bar at either 303 K or 343 K.

CO_2 - Absorption			CO_2 - Desorption		
$\frac{T}{\mathrm{K}}$	$\frac{P}{\mathrm{bar}}$	x_{CO_2}	$\frac{T}{\mathrm{K}}$	$\frac{P}{\mathrm{bar}}$	x_{CO_2}
$[P_{4,4,4,4}][2-\mathrm{ClPyCOO}]$					
1^{st} cycle					
303.13	0.0000	0.0000	303.13	0.0000	0.0000
303.14	0.2495	0.0090	303.15	0.2488	0.0115
303.16	0.4982	0.0148	303.16	0.4982	0.0191
303.15	0.7491	0.0213	303.15	0.7491	0.0262
303.14	0.9995	0.0280	303.15	1.000	0.0328
303.15	2.500	0.0646	303.13	2.499	0.0702
303.14	4.999	0.1150	303.14	4.999	0.115
312.29	0.0000	0.0000	312.29	0.0000	0.0000
313.13	0.2494	0.0045	313.12	0.2484	0.0063
313.12	0.4977	0.0103	313.12	0.4978	0.0107
313.12	0.7497	0.0140	313.14	0.7490	0.0149
313.11	0.9979	0.0174	313.11	0.9995	0.0187
313.11	2.500	0.0411	313.12	2.499	0.0428
313.13	4.999	0.0789	313.13	4.999	0.0789
320.11	0.0000	0.0000	320.16	0.0000	0.0000
323.11	0.2483	0.0059	323.12	0.2495	0.0061
323.12	0.4984	0.0092	323.10	0.4978	0.0094
323.12	0.7487	0.0115	323.12	0.7488	0.0122
323.11	0.9991	0.0135	323.11	0.9991	0.0144
323.12	2.500	0.0372	323.10	2.500	0.0367
323.12	4.998	0.0680	323.12	4.998	0.0680
336.53	0.0000	0.0000	336.53	0.0000	0.0000
343.13	0.2499	0.0052	343.08	0.2487	0.0036
343.07	0.4981	0.0065	343.04	0.4986	0.0048
343.15	0.7480	0.0065	343.09	0.7499	0.0051
343.11	0.9992	0.0078	343.08	0.9988	0.0064
343.05	2.499	0.0286	343.10	2.499	0.0282
343.05	4.998	0.0513	343.05	4.998	0.0513
$[P_{4,4,4,4}][2-\mathrm{ClPhC_1OHCOO}]$					
1^{st} cycle					
303.14	0.0000	0.0000	303.14	0.0000	0.0000
303.14	0.2492	0.0087	303.14	0.2494	0.0048
303.15	0.4974	0.0134	303.16	0.4978	0.0109
303.14	0.7488	0.0186	303.14	0.7486	0.0170
303.15	0.9992	0.0236	303.16	0.9989	0.0225
303.14	2.500	0.0545	303.13	2.499	0.0555
303.15	4.998	0.1022	303.15	4.998	0.1022
312.73	0.0000	0.0000	312.73	0.0000	0.0000

CO_2 - Absorption			CO_2 - Desorption		
$\frac{T}{K}$	$\frac{P}{bar}$	x_{CO_2}	$\frac{T}{K}$	$\frac{P}{bar}$	x_{CO_2}
313.09	0.2474	0.0033	313.09	0.2487	0.0056
313.13	0.4972	0.0101	313.14	0.4985	0.0104
313.10	0.7490	0.0142	313.12	0.7488	0.0153
313.14	0.9993	0.0180	313.11	0.9997	0.0194
313.12	2.499	0.0438	313.09	2.500	0.0455
313.10	4.998	0.0851	313.10	4.998	0.0851
318.41	0.0000	0.0000	318.41	0.0000	0.0000
323.11	0.2492	0.0061	323.12	0.2474	0.0064
323.14	0.4985	0.0100	323.14	0.4986	0.0102
323.12	0.7477	0.0125	323.13	0.7490	0.0126
323.12	0.9993	0.0149	323.12	0.9996	0.0152
323.08	2.500	0.0393	323.13	2.499	0.0399
323.13	5.000	0.0750	323.13	5.000	0.0750
335.86	0.0000	0.0000	335.86	0.0000	0.0000
343.12	0.2488	0.0048	343.11	0.2486	0.0047
343.12	0.4993	0.0055	343.09	0.4979	0.0059
343.10	0.7486	0.0070	343.09	0.7486	0.0070
343.08	0.9991	0.0108	343.12	0.9995	0.0108
343.09	2.500	0.0316	343.12	2.500	0.0326
343.06	4.999	0.0578	343.06	4.999	0.0578
$[P_{4,4,4,4}][PhSC_1COO]$					
1^{st} cycle					
320.14	0.0000	0.0000	320.14	0.0000	0.0000
323.11	0.2487	0.0041	323.12	0.2494	0.0065
323.12	0.4984	0.0099	323.11	0.4977	0.0106
323.12	0.7490	0.0126	323.12	0.7486	0.0143
323.11	1.0002	0.0155	323.12	0.9995	0.0171
323.12	2.500	0.0434	323.10	2.500	0.0441
323.12	4.999	0.0801	323.12	4.999	0.0801
337.78	0.0000	0.0000	337.78	0.0000	0.0000
343.06	0.2498	0.0047	343.12	0.2483	0.0097
343.08	0.4986	0.0048	343.10	0.4981	0.0099
343.07	0.7488	0.0078	343.10	0.7491	0.0113
343.11	0.9986	0.0119	343.09	0.9991	0.0143
343.14	2.500	0.0345	343.13	2.500	0.0359
343.37	4.999	0.0599	343.37	4.999	0.0599
$[P_{4,4,4,4}][PhC_1COO]$					
1^{st} cycle					
323.04	0.0000	0.0000	323.04	0.0000	0.0000
323.12	0.2501	0.0669	323.11	0.2491	0.0884
323.11	0.4986	0.0944	323.11	0.4986	0.1119
323.11	0.7490	0.1171	323.12	0.7470	0.1288
323.12	0.9992	0.1308	323.10	0.9999	0.1452
323.09	2.499	0.1947	323.14	2.500	0.2086
323.09	4.999	0.2540	323.10	4.999	0.254

CO_2 - Absorption			CO_2 - Desorption		
$\frac{T}{K}$	$\frac{P}{bar}$	x_{CO_2}	$\frac{T}{K}$	$\frac{P}{bar}$	x_{CO_2}
343.10	0.0000	0.0000	343.10	0.0000	0.0000
343.12	0.2490	0.0552	343.13	0.2501	0.0609
343.12	0.4981	0.0695	343.12	0.4975	0.0849
343.10	0.7490	0.0790	343.12	0.7488	0.0943
343.10	0.9992	0.0878	343.09	0.9995	0.1116
343.13	2.500	0.1312	343.15	2.498	0.1449
343.11	4.998	0.1750	343.11	4.998	0.1750
		2^{nd} cycle			
326.72	0.0000	0.0000	326.72	0.0000	0.0000
323.12	0.2495	0.0357	323.11	0.2490	0.0865
323.12	0.4990	0.0668	323.12	0.4986	0.1060
323.12	0.7490	0.0919	323.15	0.7493	0.1246
323.10	0.9991	0.1134	323.13	0.9997	0.1423
323.12	2.499	0.1738	323.10	2.500	0.2015
323.09	4.999	0.2342	323.09	4.999	0.2342
340.35	0.0000	0.0000	340.35	0.0000	0.000
343.08	0.2490	0.0522	343.06	0.2490	0.0535
343.12	0.4984	0.0658	343.11	0.4982	0.0850
343.09	0.7483	0.0744	343.12	0.7477	0.0943
343.11	0.9995	0.0818	343.11	0.9993	0.1020
343.10	2.499	0.1119	343.13	2.500	0.1290
343.14	4.998	0.1547	343.14	4.998	0.1547
		3^{rd} cycle			
343.11	0.0000	0.0000	343.11	0.0000	0.0000
343.11	0.2494	0.0496	343.10	0.2468	0.0636
343.11	0.4984	0.0633	343.09	0.4985	0.0805
343.12	0.7488	0.0717	343.11	0.7480	0.0888
343.11	0.9992	0.0794	343.10	0.9984	0.0956
343.10	2.499	0.1187	343.07	2.500	0.1235
343.08	4.999	0.1503	343.08	4.999	0.1503
		$[P_{4,4,4,4}][C_1COO]$			
339.45	0.0000	0.0000	340.35	0.0000	0.0000
343.00	0.2484	0.0516	343.10	0.2437	0.1382
343.18	0.4921	0.0870	343.13	0.5004	0.1599
343.18	0.7488	0.1084	343.13	0.7496	0.1651
343.01	0.9903	0.1221	343.04	0.9976	0.1791
343.078	2.983	0.1780	343.07	2.998	0.2057
343.07	4.993	0.2199	343.07	4.993	0.2199
		$[P_{4,4,4,4}][MeC_3COO]$			
342.44	0.0000	0.0000	334.52	0.0000	0.0000
343.11	0.2497	0.0413	343.07	0.2488	0.0465
343.09	0.4984	0.0754	343.10	0.4992	0.0817
343.14	0.7483	0.0974	343.12	0.7490	0.1015
343.09	1.0002	0.1144	343.10	0.9991	0.1214

CO_2 - Absorption			CO_2 - Desorption		
$\frac{T}{K}$	$\frac{P}{bar}$	x_{CO_2}	$\frac{T}{K}$	$\frac{P}{bar}$	x_{CO_2}
336.36	2.500	0.1814	336.44	2.498	0.1877
336.55	4.998	0.2329	336.55	4.998	0.2329
		$[P_{4,4,4,4}][c-C_6COO]$			
338.21	0.0000	0.0000	333.25	0.0000	0.0000
343.11	0.2501	0.0335	336.91	0.2487	0.0384
343.13	0.4986	0.0541	343.14	0.4990	0.0567
343.12	0.7468	0.0691	343.09	0.7483	0.0714
343.11	0.9996	0.0828	343.09	0.9979	0.0865
343.14	2.499	0.1338	343.13	2.499	0.1355
343.11	4.998	0.1800	343.11	4.998	0.1800
		$[P_{4,4,4,4}][C_5COO]$			
325.87	0.0000	0.0000	331.59	0.0000	0.0000
343.16	0.2495	0.0406	343.14	0.2498	0.0494
343.14	0.4984	0.0705	340.23	0.4966	0.0831
343.14	0.7488	0.0912	343.15	0.7490	0.1030
343.16	0.9999	0.1075	336.83	0.9997	0.1402
343.14	4.998	0.2145	343.14	4.998	0.2145
		$[P_{4,4,4,4}][C_{11}COO]$			
		1^{st} cycle			
330.73	0.0000	0.0000	303.15	0.0000	0.0000
303.17	0.2494	0.0093	303.15	0.2488	0.0202
303.13	0.4981	0.0166	303.14	0.4990	0.0257
303.19	0.7486	0.0244	303.15	0.7490	0.0315
303.13	0.9993	0.0320	303.16	1.0002	0.0374
303.14	2.499	0.0728	303.07	2.499	0.0760
303.12	4.998	0.1343	303.12	4.998	0.1343
331.79	0.0000	0.0000	331.22	0.0000	0.0000
343.16	0.2484	0.0616	343.15	0.2494	0.0871
343.15	0.4981	0.0932	343.16	0.4981	0.1118
343.16	0.7486	0.1159	343.19	0.7491	0.1291
343.12	0.9982	0.1341	343.15	1.0000	0.1475
343.19	2.499	0.1913	343.14	2.498	0.1993
343.29	4.999	0.2479	343.29	4.999	0.2479
		2^{nd} cycle			
303.13	0.0000	0.0000	303.13	0.0000	0.0000
303.15	0.2492	0.0089	303.16	0.2490	0.0176
303.14	0.4982	0.0167	303.14	0.4979	0.0238
303.16	0.7491	0.0242	303.15	0.7488	0.0298
303.16	0.9986	0.0317	303.11	0.9986	0.036
303.15	2.500	0.0722	303.14	2.500	0.0746
303.14	4.998	0.1330	303.14	4.998	0.1330
340.35	0.0000	0.0000	340.35	0.0000	0.0000
343.12	0.2491	0.0634	343.11	0.2491	0.0691
343.11	0.4979	0.0914	343.11	0.4981	0.0955

CO_2 - Absorption			CO_2 - Desorption		
$\frac{T}{K}$	$\frac{P}{bar}$	x_{CO_2}	$\frac{T}{K}$	$\frac{P}{bar}$	x_{CO_2}
343.12	0.7486	0.1088	343.18	0.7479	0.1167
343.09	0.9984	0.1245	336.92	0.9996	0.1418
343.11	2.499	0.1854	343.11	2.499	0.1873
343.09	4.998	0.2362	343.09	4.998	0.2362
			$[P_{6,6,6,14}][C_{11}COO]$		
299.87	0.0000	0.0000	303.16	0.0000	0.0000
303.15	0.2492	0.0803	303.14	0.2494	0.0938
303.14	0.4993	0.0924	303.15	0.4982	0.1111
303.14	0.7488	0.1050	303.15	0.7483	0.1214
303.15	0.9989	0.1162	303.18	0.9993	0.1296
303.14	2.500	0.1665	303.15	2.498	0.1734
303.15	4.999	0.2349	303.15	4.999	0.2349
336.95	0.0000	0.0000	327.27	0.0000	0.0000
343.12	0.2481	0.0766	343.12	0.2491	0.0787
343.11	0.4938	0.0992	343.13	0.4970	0.1062
337.43	0.7475	0.1175	343.12	0.7487	0.1189
343.11	0.9991	0.1305	343.10	0.9992	0.1346
343.12	2.499	0.1859	343.11	2.499	0.1894
343.08	4.999	0.2435	343.08	4.999	0.2435
			$[P_{4,4,4,4}][Me_4C_4COO]$		
			1^{st} cycle		
303.21	0.0000	0.0000	303.21	0.0000	0.0000
303.15	0.2497	0.3074	303.19	0.2494	0.4045
303.12	0.4984	0.4015	303.17	0.4979	0.4341
303.16	0.7493	0.4419	303.14	0.7494	0.4452
303.16	0.9991	0.4578	303.12	0.9988	0.4522
303.16	2.498	0.4897	303.13	2.498	0.4904
303.16	4.999	0.5129	303.16	4.999	0.5129
323.12	0.0000	0.0000	323.12	0.0000	0.0000
323.10	0.2488	0.1911	323.11	0.2497	0.2382
323.11	0.4985	0.2979	323.11	0.4971	0.2917
323.12	0.7487	0.3448	323.12	0.7490	0.3120
323.11	0.9991	0.3602	323.13	0.9995	0.3236
323.09	2.498	0.4176	323.11	2.501	0.4019
323.14	4.993	0.4555	323.14	4.993	0.4555
343.03	0.0000	0.0000	343.03	0.0000	0.0000
343.13	0.2491	0.0788	343.08	0.2490	0.0720
343.12	0.4993	0.1220	343.13	0.4988	0.1107
343.10	0.7476	0.1498	343.20	0.7459	0.1301
343.08	0.9989	0.1670	343.10	0.9985	0.1396
343.07	2.497	0.2401	343.04	2.498	0.2252
343.16	4.996	0.2871	343.16	4.996	0.2871
			2^{nd} cycle		
341.60	0.0000	0.0000	341.60	0.0000	0.0000
343.12	0.2491	0.0915	343.10	0.2497	0.0962

CO_2 - Absorption			CO_2 - Desorption		
$\frac{T}{\mathrm{K}}$	$\frac{P}{\mathrm{bar}}$	x_{CO_2}	$\frac{T}{\mathrm{K}}$	$\frac{P}{\mathrm{bar}}$	x_{CO_2}
343.12	0.4988	0.1270	343.11	0.4984	0.1283
343.09	0.7480	0.1504	343.12	0.7490	0.1521
343.14	0.9995	0.1695	343.14	0.9978	0.1706
343.14	2.499	0.2390	336.54	2.499	0.2624
343.09	4.998	0.2833	343.09	4.998	0.2833
$[P_{6,6,6,14}][Me_4C_4COO]$					
1^{st} cycle					
303.52	0.0000	0.0000	303.52	0.0000	0.0000
303.11	0.2491	0.0721	303.15	0.2498	0.0829
303.18	0.4984	0.0882	303.17	0.4982	0.0993
303.15	0.7487	0.1009	303.14	0.7477	0.1101
303.15	0.9995	0.1118	303.14	0.9989	0.1188
303.15	2.500	0.1586	303.15	2.498	0.1617
303.15	4.999	0.2202	303.15	4.999	0.2202
318.54	0.0000	0.0000	318.54	0.0000	0.0000
323.16	0.2985	0.1011	323.06	0.4975	0.1243
323.17	0.7490	0.1127	323.17	0.7469	0.1339
323.18	0.9989	0.1237	323.16	1.0003	0.1419
323.15	2.499	0.1695	323.15	2.499	0.1817
323.16	4.999	0.2268	323.16	4.999	0.2268
334.22	0.0000	0.0000	334.22	0.0000	0.0000
342.65	0.2504	0.0833	343.10	0.2492	0.0851
343.35	0.4979	0.1078	343.08	0.4979	0.1088
343.08	0.7486	0.1232	343.12	0.7490	0.1245
343.18	0.9993	0.1363	343.13	0.9988	0.1389
342.93	2.499	0.1966	343.14	2.500	0.2139
342.99	4.997	0.2528	342.99	4.997	0.2528
2^{nd} cycle					
303.14	0.0000	0.0000	303.14	0.0000	0.0000
303.14	0.2488	0.0735	303.14	0.2491	0.0788
303.14	0.4975	0.0931	303.15	0.4992	0.0976
303.14	0.7476	0.1073	303.15	0.7488	0.1110
303.13	0.9992	0.1190	303.18	0.9989	0.1218
303.15	2.499	0.1684	303.15	2.500	0.1696
303.15	4.999	0.2292	303.15	4.999	0.2292
333.39	0.0000	0.0000	333.39	0.0000	0.0000
343.14	0.2494	0.1200	343.14	0.2490	0.1203
343.07	0.4979	0.1420	343.20	0.4971	0.1414
343.20	0.7481	0.1568	343.24	0.7487	0.1566
343.23	0.9986	0.1696	343.08	0.9999	0.1695
343.16	2.500	0.2223	343.18	2.500	0.2289
343.13	4.998	0.2761	343.13	4.998	0.2761

3 CO_2 absorption model

$$K_H = \lim_{x_{CO_2} \to 0} \frac{\phi_{CO_2} P}{x_{CO_2}} \approx \frac{P}{x_{CO_2}} \tag{S2}$$

Compound	n_i
CO_2 (sol)	$n_{CO_2}(1-\xi)$
$[P_{4,4,4,4}][RCOO]$	$n_{IL} - 2n_{CO_2}\xi$
$[P^+_{4,4,4,4}\text{-}CO_2^-]$	$n_{CO_2}\xi$
$[P_{4,4,4,4}][RCOO]$ - - HOOCR	$n_{CO_2}\xi$
Total	$n_{CO_2}(1-\xi) + n_{IL}$

$$K_{eq,1:2} = \frac{\gamma_{zwi}\gamma_{compl}}{\gamma_{CO_2}\gamma_{IL}} \frac{x_{zwi}x_{compl}}{x_{CO_2}x_{IL}^2}$$
$$K_{eq,1:2} \approx \frac{x_{zwi}x_{compl}}{x_{CO_2}x_{IL}^2} \tag{S3}$$
$$K_{eq,1:2} = \frac{n_{CO_2}\xi^2[n_{CO_2}(1-\xi) + n_{IL}]}{(1-\xi)(n_{IL} - 2n_{CO_2}\xi)^2}$$

where γ_{zwi}, γ_{compl}, γ_{CO_2}, and γ_{IL} represent the activity coefficients, while x_{zwi}, x_{compl}, x_{CO_2}, and x_{IL} denote the mole fractions of the zwitterion, complex, dissolved CO_2, and neat IL in Equation S3 , respectively. In Equation S2, ϕ_{CO_2} corresponds to the fugacity coefficient of CO_2, and P represents the equilibrium pressure of the system. Ideal solutions are assumed, implying that the activity coefficients are concentration-independent and are thus incorporated into the K_{eq} value. is considered ideal ($\phi_{CO_2} \approx 1$). The K_{eq} equation is reformulated as a function of the compound amounts, taking into account the extent of reaction ξ.

Table S13 – Henry's law constant (K_H) and the equilibrium constant (K_{eq}) obtained for various ILs by fitting the data in Table S12 of the successive cycles at either 303 K, 323 K or 343 K.

Sample	Cycle	$\frac{T}{K}$	K_{eq}	$\frac{K_H}{bar}$
$[P_{4,4,4,4}][PhC_1COO]$	2nd	323	0.8 ± 0.2	45 ± 4
	2nd	343	1.2 ± 0.2	139 ± 29
	3rd	343	1.2 ± 0.3	144 ± 35
$[P_{4,4,4,4}][C_{11}COO]$	2nd	303		36.4 ± 0.8
	2nd	343	1.8 ± 0.3	59 ± 4
$[P_{4,4,4,4}][Me_4C_4COO]$	2nd	343	5 ± 1	53 ± 6
$[P_{6,6,6,14}][Me_4C_4COO]$	2nd	303	1.3 ± 0.2	58 ± 3
	2nd	343	5.3 ± 0.5	58 ± 2

4 NMR before and after CO_2 absorption

4.1 $[P_{4,4,4,4}][2-ClPyCOO]$

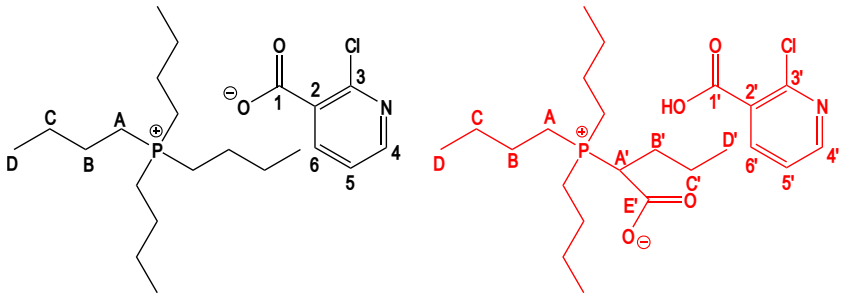

Figure S12 – Chemical structure of the $[P_{4,4,4,4}][2-ClPyCOO]$ (left) before and (right) after CO_2 absorption.

Tetrabutylphosphonium 2-chloropyridine-3-carboxylate $[P_{4,4,4,4}][2-ClPyCOO]$ after CO_2 absorption: ^{1}H NMR (400 MHz, C_6D_6, 343 K) δ ppm: 0.73 (m, 12H, D); 1.25 (m, 8H, C); 1.41 (m, 8H, B); 2.35 (m, 8H, A); 7.14 (t, 1H, 5); 7.63 (d, 1H, 6); 8.02 (m, 1H, 4). ^{13}C NMR (100 MHz, C_6D_6, 343 K) δ ppm: 12.41 (4C, D); 17.57 (4C, A); 22.71 (7C, B); 22.89 (4C, C); 121.54 (1C, 5); 136.33 (1C, 6); 139.72 (1C, 2); 145.58 (1C, 4); 146.45 (1C, 3); 166.03 (1C, 1). ^{31}P NMR (161 MHz, C_6D_6, 343 K) δ ppm: 33.65 (1P, $\mathbf{P}((CH_2)_3CH_3)_4$).

4.2 $[P_{4,4,4,4}][2-ClPhC_1OHCOO]$

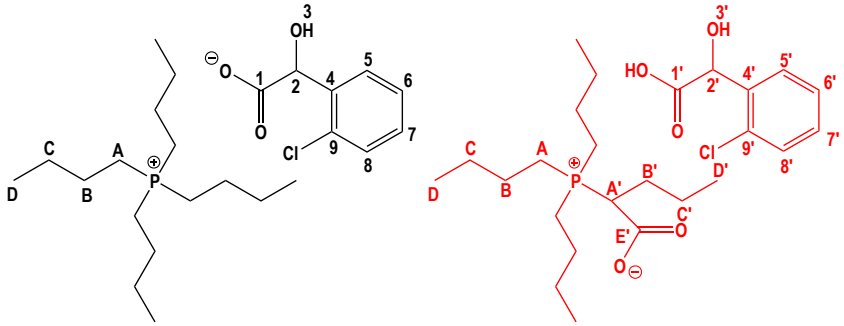

Figure S13 – Chemical structure of the $[P_{4,4,4,4}][2-ClPhC_1OHCOO]$ (left) before and (right) after CO_2 absorption.

Tetrabutylphosphonium 2-(2-chlorophenylacetate)-2-hydroxyacetate $[P_{4,4,4,4}][2-ClPhC_1OHCOO]$ after CO_2 absorption: ^{1}H NMR (400 MHz, C_6D_6, 343 K) δ ppm: 0.73 (t, 12H, $^{3}J_{HH} = 6.8$ Hz, D); 1.22 (m, 16H, B+C); 2.05 (m, 8H, A); 4.81 (s, 1H, 2); 5.56 (s, 1H, 3); 6.96 (m, 2H, 7+8); 7.06 (m, 1H,

5); 7.26 (m, 1H, 6). ^{13}C NMR (100 MHz, C_6D_6, 343 K) δ ppm: 12.33 (4C, D); 17.35 (4C, A); 22.51 (4C, B); 22.80 (4C, C); 70.11 (1C, 2); 125.24 (1C, 7); 126.28 (1C, 8); 127.55 (1C, 6); 127.76 (1C, 5); 132.79 (1C, 4); 142.60 (1C, 9); 171.90 (1C, 1). ^{31}P NMR (161 MHz, C_6D_6, 343 K) δ ppm: 33.22 (1P, **P**$((CH_2)_3CH_3)_4$). 3

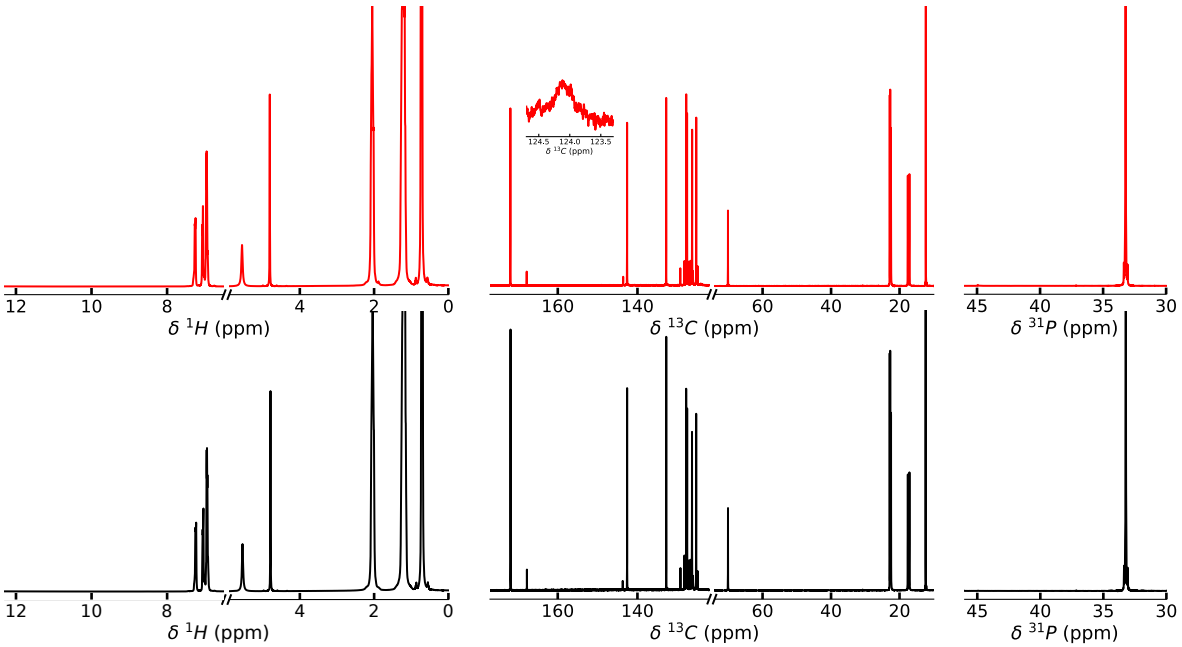

Figure S14 – (Left) ^{1}H, (middle) ^{13}C and (right) ^{31}P NMR spectra of $[P_{4,4,4,4}][2-ClPhC_1OHCOO]$ — before and — after CO_2 absorption at 343 K.

4.3 $[P_{4,4,4,4}][PhSC_1COO]$

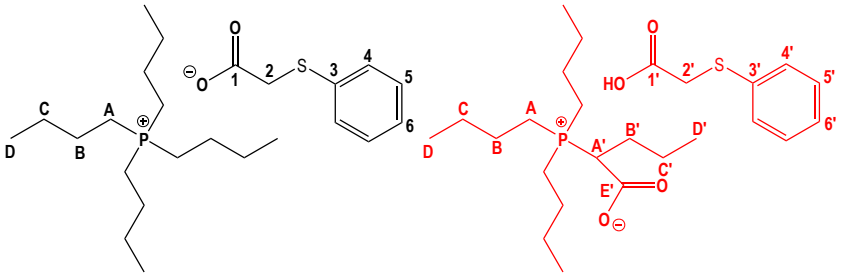

Figure S15 – Chemical structure of the $[P_{4,4,4,4}][PhSC_1COO]$ (left) before and (right) after CO_2 absorption.

Tetrabutylphosphonium (thiophenyl)acetate $[P_{4,4,4,4}][PhSC_1COO]$ after CO_2 absorption: ^{1}H NMR (400 MHz, C_6D_6, 343 K) δ ppm: 0.77 (t, 12H, $^{3}J_{HH}$ = 7.8 Hz, D); 1.30 (m, 8H, C); 1.38 (m, 8H, B); 2.34 (m, 8H, A); 3.36 (s, 1H, 2); 6.87 (t, 1H, $^{3}J_{HH}$ = 7.2 Hz, 6); 7.02 (m, 2H, $^{3}J_{HH}$ = 7.5 Hz, 5); 7.15 (d, 2H, $^{3}J_{HH}$ = 7.1 Hz, 4). ^{13}C NMR (100 MHz, C_6D_6, 343 K) δ ppm: 13.79 (4C, D); 18.88 (4C, A); 24.11,

24.29 (8C, B+C); 41.38 (1C, 2); 124.35 (1C, 6); 127.24 (2C, 4); 128.78 (2C, 5); 141.42 (1C, 3); 168.77 (1C, 1). ^{31}P NMR (161 MHz, C_6D_6, 343 K) δ ppm: 33.47 (1P, **P**$((CH_2)_3CH_3)_4$).

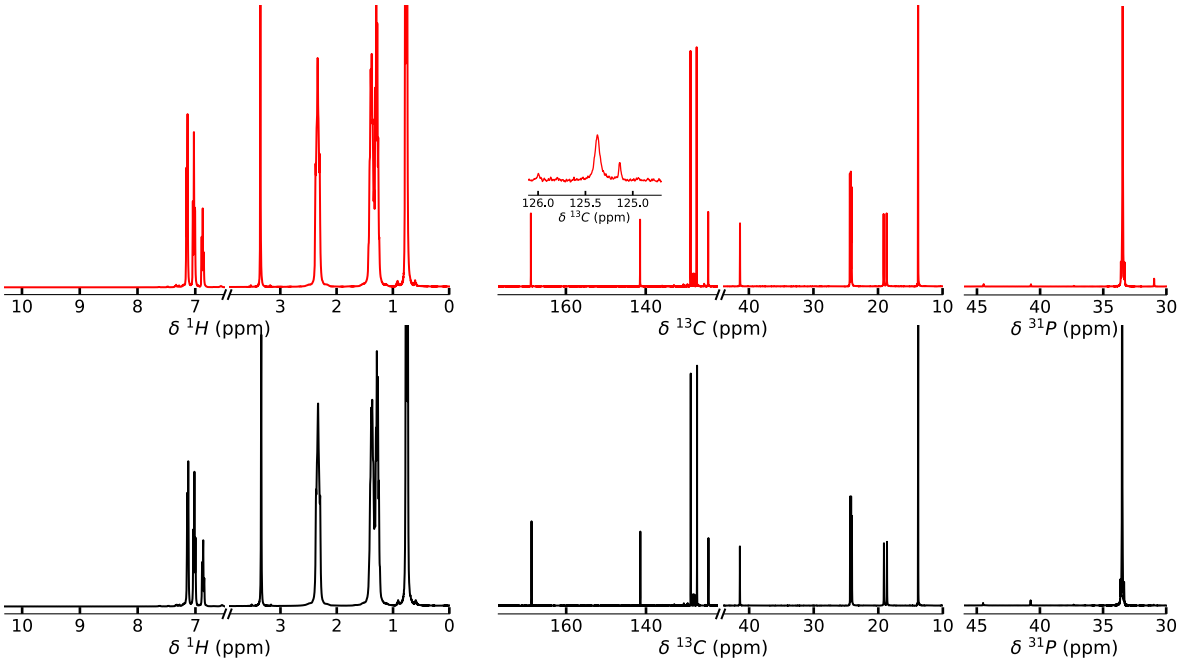

Figure S16 – (Left) ^{1}H, (middle) ^{13}C and (right) ^{31}P NMR spectra of [$P_{4,4,4,4}$][$PhSC_1COO$] — before and — after CO_2 absorption at 343 K.

4.4 [$P_{4,4,4,4}$][PhC_1COO]

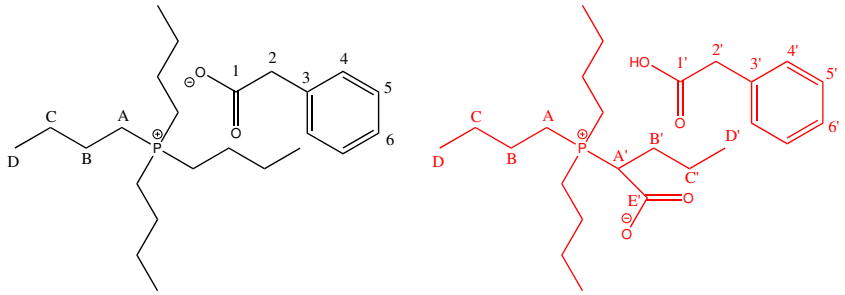

Figure S17 – Chemical structure of the [$P_{4,4,4,4}$][PhC_1COO] (left) before and (right) after CO_2 absorption.

Tetrabutylphosphonium phenylacetate [$P_{4,4,4,4}$][PhC_1COO] after CO_2 absorption: ^{1}H NMR (400 MHz, DMSO-d_6, 343 K) δ ppm: 0.97 (t, 12H, $^{3}J_{HH} = 6.8$ Hz, D+D'); 1.40-1.56 (m, 14H, B+B'+C+C'); 1.96 (m, 2H, B'); 2.26 (m, 6H, A); 2.35 (m, 8H, A); 2.87 (t, 1H, $^{3}J_{HH} = 11.8$ Hz, A'); 3.48 (s, 2H, 2'); 7.14 (t, 1H, $^{3}J_{HH} = 7.3$ Hz, 6'); 7.23 (t, 2H, $^{3}J_{HH} = 7.4$ Hz, 5'); 7.37 (d, 2H, $^{3}J_{HH} = 7.5$ Hz, 4'); 14.12 (1H, RCOO**H**). ^{13}C NMR (100 MHz, DMSO-d_6, 343 K) δ ppm: 12.28 (3C, D); 12.31 (4C,

D); 12.69 (1C, D'); 17.35 (4C, A); 18.10 (3C, A); 21.33 (1C, C'); 22.41-23.10 (7C, B+C+C'); 28.38 (1C, B'); 40.98 (1C, A'); 44.74 (1C, 2'); 124.09 (1C, 6'); 126.57 (2C, 5'); 128.46 (2C, 4'); 138.97 (1C, 3'); 165.36 (1C, E'); 172.49 (1C, 1'). ^{31}P NMR (161 MHz, DMSO-d_6, 343 K) δ ppm: 31.25 (1P, **P**($CHCO_2(CH_2)_2CH_3$)($(CH_2)_3CH_3$)$_3$); 33.57 (1P, **P**($(CH_2)_3CH_3$)$_4$).

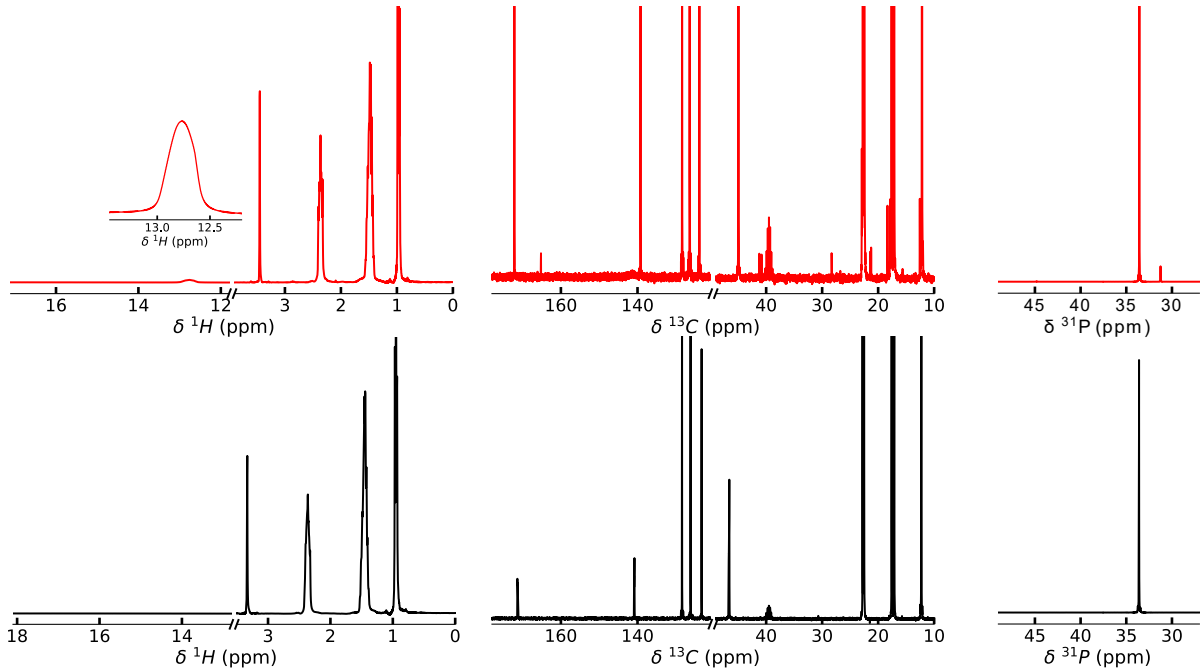

Figure S18 – (Left) ^{1}H, (middle) ^{13}C and (right) ^{31}P NMR spectra of [$P_{4,4,4,4}$][PhC_1COO] — before and — after CO_2 absorption at 343 K.

4.5 [$P_{4,4,4,4}$][C_1COO]

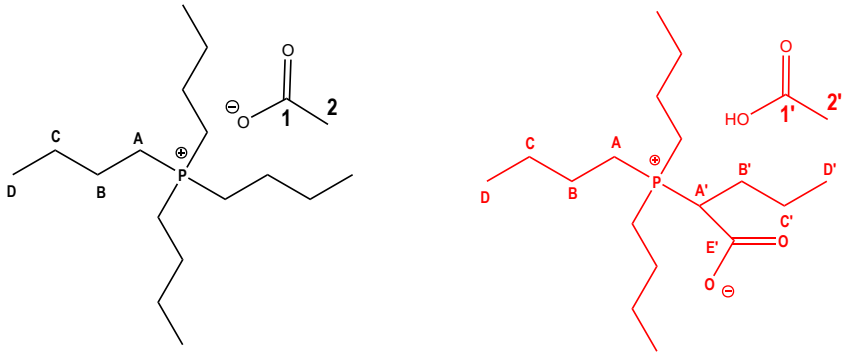

Figure S19 – Chemical structure of the [$P_{4,4,4,4}$][C_1COO] (left) before and (right) after CO_2 absorption.

Tetrabutylphosphonium acetate [$P_{4,4,4,4}$][C_1COO] after CO_2 absorption: ^{1}H NMR (400 MHz, C_6D_6, 343 K) δ ppm: 0.99 (t, 12H, $^{3}J_{HH}$ = 6.9 Hz, D + D'); 1.53 (m, 8H, C + C'); 1.64 (m, 8H, B + B'); 1.82

(m, 2H, 2'); 2.42 (m, 6H, A); 2.54 (m, 8H, A); 2.87 (t, 1H, $^{3}J_{HH}$ = 11.1 Hz, A'); 15.86 (1H, RCOO**H**). ^{13}C NMR (100 MHz, C_6D_6, 343 K) δ ppm: 13.71 (4C, D); 14.10 (1C, D'); 18.91 (4C, A); 19.60 (3C, A); 24.11 (8C, B+B'); 24.27 (8C, C+C'); 24.42 (1C, 2'); 42.64 (1C, A'); 166.82 (1C, E'); 173.68 (1C, 1'). ^{31}P NMR (161 MHz, C_6D_6, 343 K) δ ppm: 31.18 (1P, **P**($CHCO_2(CH_2)_2CH_3$)($(CH_2)_3CH_3$)$_3$); 33.66 (1P, **P**($(CH_2)_3CH_3$)$_4$).

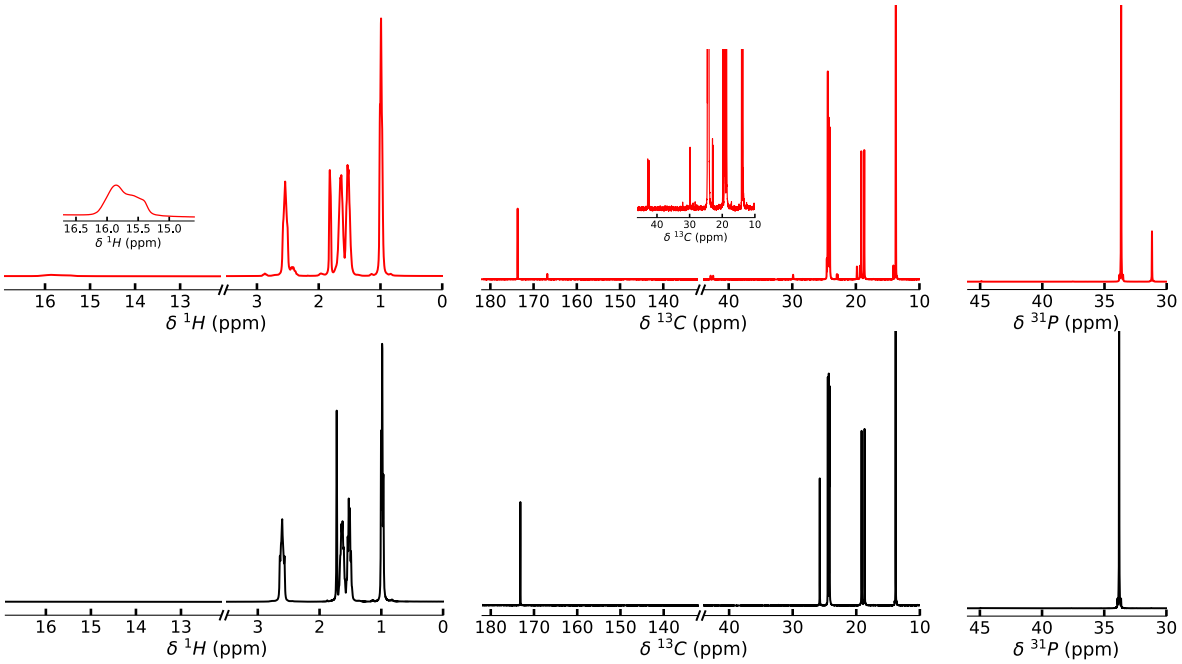

Figure S20 – (Left) ^{1}H, (middle) ^{13}C and (right) ^{31}P NMR spectra of $[P_{4,4,4,4}][C_1COO]$ — before and — after CO_2 absorption at 343 K.

4.6 $[P_{4,4,4,4}][MeC_3COO]$

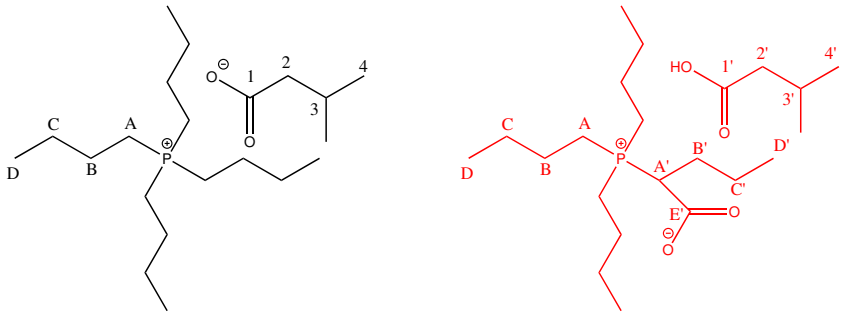

Figure S21 – Chemical structure of the $[P_{4,4,4,4}][MeC_3COO]$ (left) before and (right) after CO_2 absorption.

Tetrabutylphosphonium isovalerate $[P_{4,4,4,4}][MeC_3COO]$ after CO_2 absorption: ^{1}H NMR (400 MHz, C_6D_6, 343 K) δ ppm: 0.94 (d, 6H, $^{3}J_{HH}$ = 6.4 Hz, 4'); 0.97 (t, 12H, $^{3}J_{HH}$ = 7.3 Hz, D + D'); 1.51 (m,

8H, C + C'); 1.62 (m, 8H, B + B'); 1.99 (m, 2H, 2'); 2.05 (m, 1H, 3'); 2.44 (m, 6H, A); 2.57 (m, 8H, A); 2.85 (t, 1H, $^{3}J_{HH}$ = 11.7 Hz, A'); 17.52 (1H, RCOO**H**). ^{13}C NMR (100 MHz, C_6D_6, 343 K) δ ppm: 13.64 (3C, D); 13.68 (4C, D); 14.06 (1C, D'); 19.19 (4C, A); 19.86 (3C, A); 23.27 (1C, C'): 23.44 (2C, 4'); 24.18-24.66 (7C, B+C+C'); 26.58 (1C, 3'); 29.97 (1C, B'); 42.74 (1C, A'); 48.03 (1C, 2'); 166.68 (1C, E'); 175.42 (1C, 1'). ^{31}P NMR (161 MHz, C_6D_6, 343 K) δ ppm: 31.23 (1P, **P**($CHCO_2(CH_2)_2CH_3$)($(CH_2)_3CH_3$)$_3$); 33.75 (1P, **P**($(CH_2)_3CH_3$)$_4$).

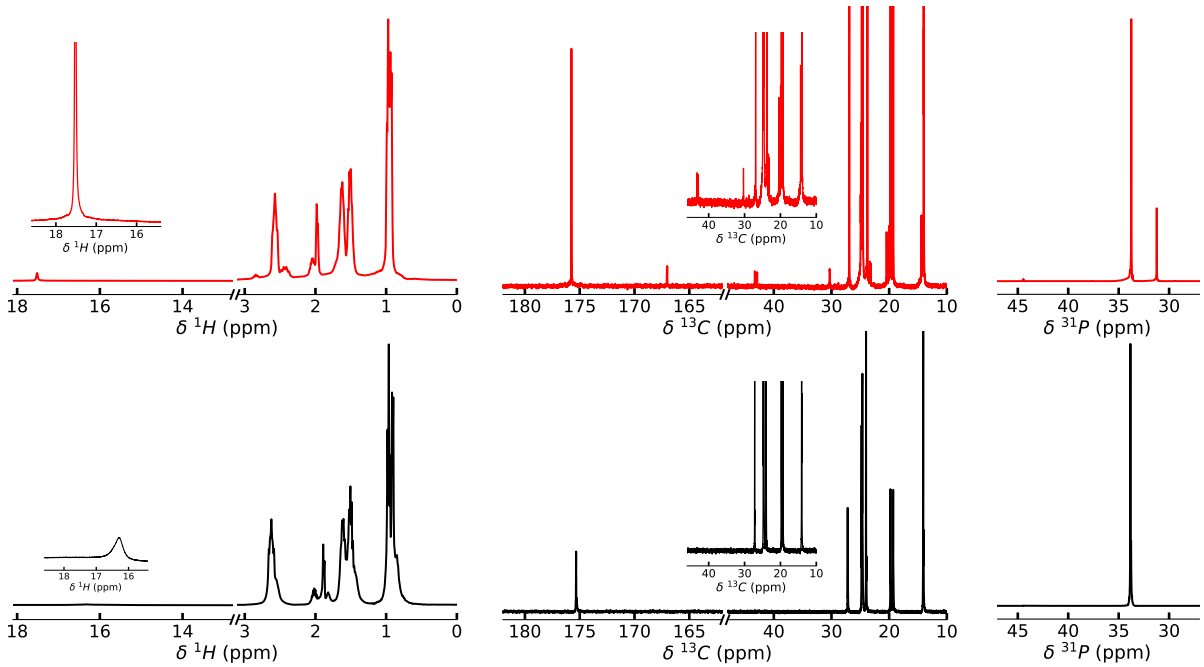

Figure S22 – (Left) ^{1}H, (middle) ^{13}C and (right) ^{31}P NMR spectra of [$P_{4,4,4,4}$][MeC_3COO] — before and — after CO_2 absorption at 343 K.

4.7 [$P_{4,4,4,4}$][c−C_6COO]

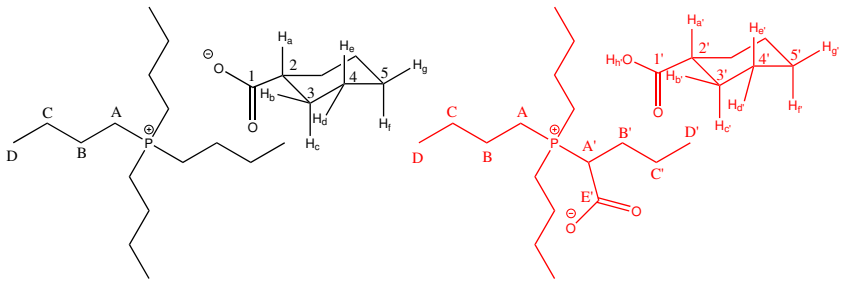

Figure S23 – Chemical structure of the [$P_{4,4,4,4}$][c−C_6COO] (left) before and (right) after CO_2 absorption.

Tetrabutylphosphonium cyclohexanecarboxylate [$P_{4,4,4,4}$][c−C_6COO] after CO_2 absorption: ^{1}H NMR (400 MHz, C_6D_6, 343 K) δ ppm: 0.94 (m, 12H, D+D'); 1.20 (m, 1H, 5', $H_{f'}$); 1.24 (m, 2H, 4',

$H_{e'}$); 1.38 (m, 2H, 5', $H_{c'}$); 1.48 (m, 8H, C+C'); 1.57 (m, 1H, 5', $H_{g'}$); 1.58 (m, 8H, B+B'); 1.66 (m, 2H, 4', $H_{d'}$); 1.82 (m, 2H, 3', $H_{b'}$); 2.02 (m, 1H, 2', $H_{a'}$); 2.55 (m, 6H, A); 2.81 (t, 1H, $^{3}J_{HH}$ = 11.2 Hz, A'); 16.04 (1H, RCOO**H**). ^{13}C NMR (100 MHz, C_6D_6, 343 K) δ ppm: 13.58 (3C, D); 13.63 (4C, D); 13.97 (1C, D'); 19.17 (4C, A); 19.81 (3C, A); 24.04-24.60 (6C, B+C+C'); 26.76 (2C, 4'); 27.20 (1C, 5'); 29.91 (1C, B'); 31.06 (2C, 3'); 42.89 (1C, A'); 46.36 (1C, 2'); 166.65 (1C, E'); 178.57 (1C, 1'). ^{31}P NMR (161 MHz, C_6D_6, 343 K) δ ppm: 31.11 (1P, **P**($CHCO_2(CH_2)_2CH_3$)($(CH_2)_3CH_3$)$_3$); 33.56 (1P, **P**($(CH_2)_3CH_3$)$_4$).

4.8 [$P_{4,4,4,4}$][C_5COO]

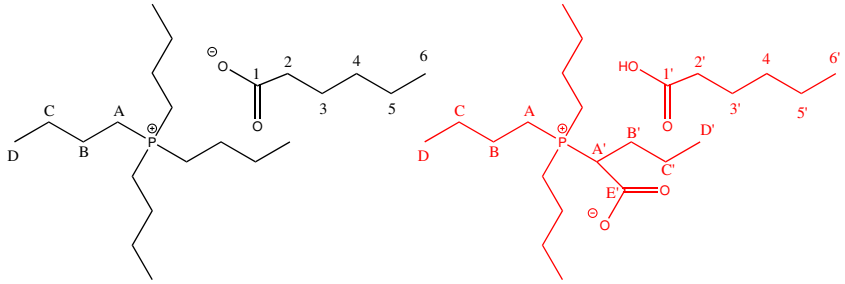

Figure S24 – Chemical structure of the [$P_{4,4,4,4}$][C_{11}COO] (left) before and (right) after CO_2 absorption.

Tetrabutylphosphonium hexanoate [$P_{4,4,4,4}$][C_5COO] after CO_2 absorption: ^{1}H NMR (400 MHz, C_6D_6, 343 K) δ ppm: 0.93 (m, 3H, 6'); 1.00 (m, 12H, D+D'); 1.35 (m, 4H, 4'+5'); 1.54 (m, 8H, C + C'); 1.58 (m, 2H, 3'); 1.65 (m, 8H, B+B'); 2.09 (t, 2H, $^{3}J_{HH}$ = 7.6 Hz, 2'); 2.45 (m, 6H, A); 2.62 (m, 8H, A); 2.87 (t, 1H, $^{3}J_{HH}$ = 11.5 Hz, A'); 16.92 (1H, RCOO**H**). ^{13}C NMR (100 MHz, C_6D_6, 343 K) δ ppm: 13.68 (3C, D); 13.73 (4C, D); 14.08 (1C, D'); 14.31 (1C, 6'); 19.04 (4C, A); 19.74 (3C, A); 23.09 (1C, 5'); 24.17-24.39 (3C, B); 24.39-24.68 (4C, C+C'); 26.78 (1C, 3'); 29.95 (1C, B'); 37.71 (1C, 4'); 38.26 (1C, 2'); 42.61 (1C, A'); 166.75 (1C, E'); 176.12 (1C, 1'). ^{31}P NMR (161 MHz, C_6D_6, 343 K) δ ppm: 31.17 (1P, **P**($CHCO_2(CH_2)_2CH_3$)($(CH_2)_3CH_3$)$_3$); 33.69 (1P, **P**($(CH_2)_3CH_3$)$_4$).

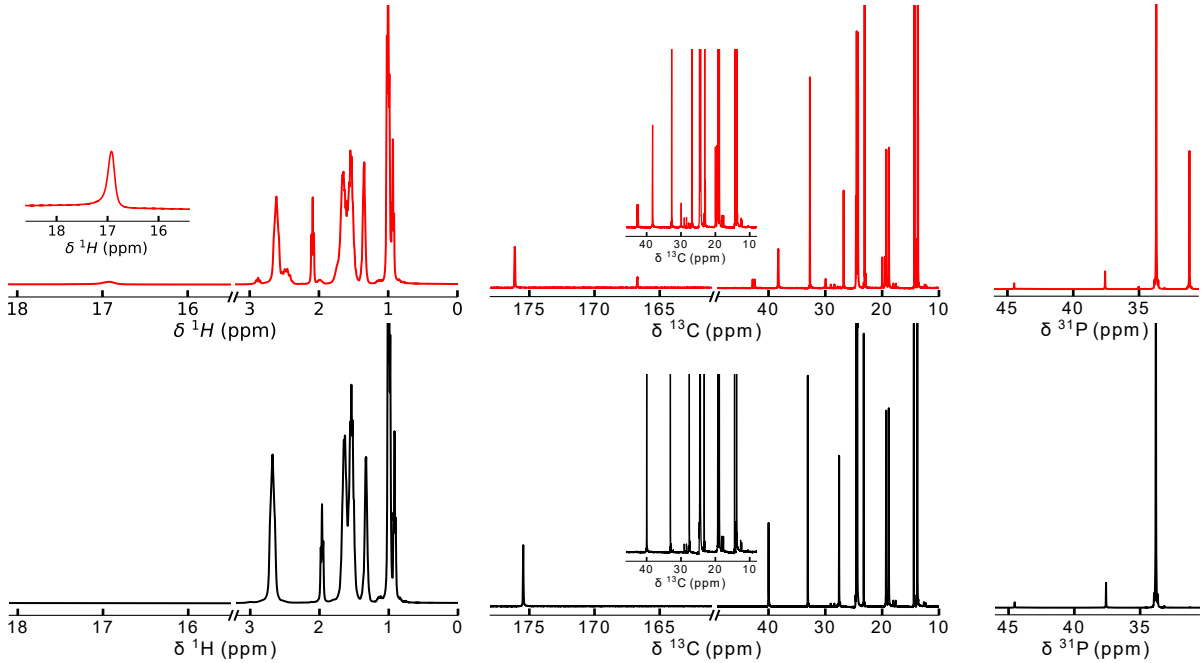

Figure S25 – (Left) ^{1}H, (middle) ^{13}C and (right) ^{31}P NMR spectra of [$P_{4,4,4,4}$][C_5COO] — before and — after CO_2 absorption at 343 K.

4.9 [$P_{4,4,4,4}$][C_{11}COO]

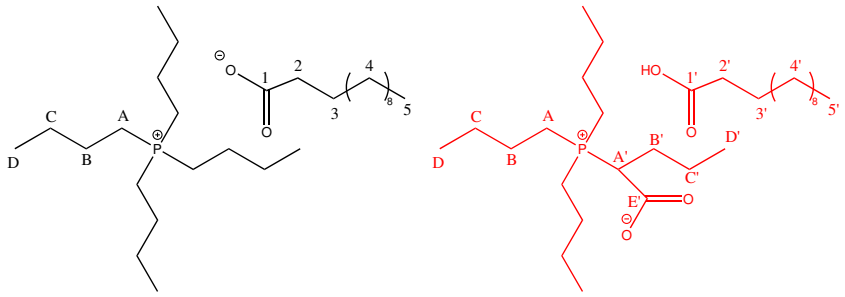

Figure S26 – Chemical structure of the [$P_{4,4,4,4}$][C_{11}COO] (left) before and (right) after CO_2 absorption.

Tetrabutylphosphonium dodecanoate [$P_{4,4,4,4}$][C_{11}COO] after CO_2 absorption: ^{1}H NMR (400 MHz, C_6D_6, 343 K) δ ppm: 0.93 (t, 3H, $^{3}J_{HH}$ = 6.1 Hz, 5'); 1.00 (t, 12H, $^{3}J_{HH}$ = 7.4 Hz, D+D'); 1.33 (m, 18H, 4'); 1.55 (m, 8H, C + C'); 1.59 (m, 2H, 3'); 1.66 (m, 8H, B+B'); 2.10 (t, 2H, $^{3}J_{HH}$ = 7.2 Hz, 2'); 2.45 (m, 6H, A); 2.60 (m, 8H, A); 2.88 (t, 1H, $^{3}J_{HH}$ = 11.5 Hz, A'); 17.04 (1H, RCOO**H**). ^{13}C NMR (100 MHz, C_6D_6, 343 K) δ ppm: 13.60 (3C, D); 13.66 (4C, D); 14.00 (1C, D'); 14.17 (1C, 5'); 19.21 (4C, A); 19.91 (3C, A); 22.98, 29.62-30.48, 32.31 (8C, 4'); 24.19-24.68 (7C, B+C+C'); 27.09 (1C, 3'); 30.29 (1C, B'); 38.19 (1C, 2'); 42.62 (1C, A'); 166.68 (1C, E'); 176.20 (1C, 1'). ^{31}P NMR (161 MHz, C_6D_6,

343 K) δ ppm: 31.22 (1P, **P**($CHCO_2(CH_2)_2CH_3$)($(CH_2)_3CH_3$)$_3$); 33.71 (1P, **P**($(CH_2)_3CH_3$)$_4$).

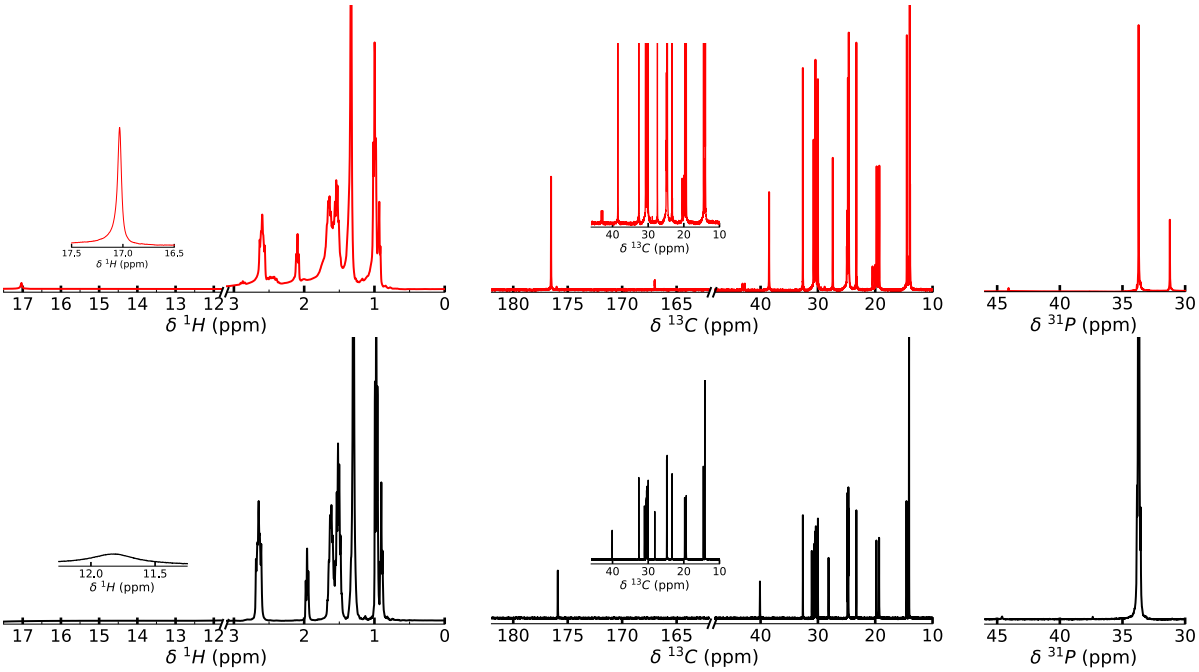

Figure S27 – (Left) ^{1}H, (middle) ^{13}C and (right) ^{31}P NMR spectra of [$P_{4,4,4,4}$][$C_{11}COO$] — before and — after CO_2 absorption at 343 K.

4.10 [$P_{6,6,6,14}$][$C_{11}COO$]

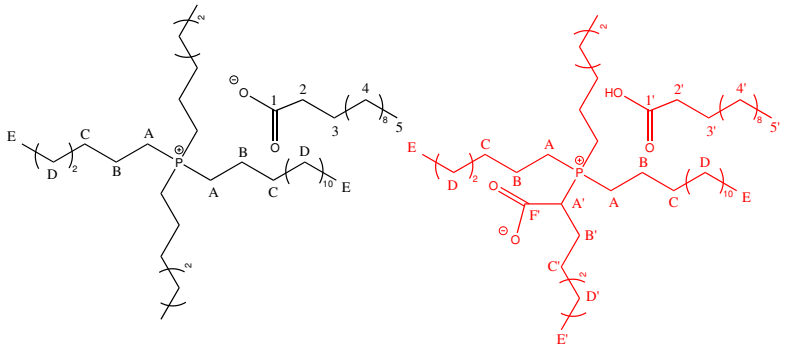

Figure S28 – Chemical structure of the [$P_{6,6,6,14}$][$C_{11}COO$] (left) before and (right) after CO_2 absorption. For the sack of clarity, the CO_2 absorbed has been represented on one of the hexyl alkyl chain of the phosphonium cation, but it also could be grafted on the tetradecyl alkyl chain without any clear preference.

Trihexyltetradecylphosphonium dodecanoate [$P_{6,6,6,14}$][$C_{11}COO$] after CO_2 absorption: ^{1}H NMR (400 MHz, C_6D_6, 343 K) δ ppm: 0.94-1.02 (m, 15H, 5'+E+E'); 1.34-1.46 (m, 48H, D+D'+4'); 1.56 (m, 8H, C + C'); 1.63 (m, 2H, 3'); 1.69 (m, 8H, B+B'); 2.15 (t, 2H, $^3J_{HH}$ = 7.3 Hz, 2'); 2.45 (m, 6H, A); 2.64 (m, 8H, A); 2.88 (t, 1H, $^3J_{HH}$ = 11.4 Hz, A'); 14.40 (1H, RCOO**H**). ^{13}C NMR (100 MHz,

C_6D_6, 343 K) δ ppm: 14.26 (5C, E+E'+5'); 19.50 (4C, A); 20.24 (3C, A); 22.31 (3C, B); 22.87, 23.06, 29.44-32.44 (24C, D+D'+4'); 30.82 (1C, B'); 31.01 (4C, C+C'); 26.89 (1C, 3'); 37.70 (1C, 2'); 42.49 (1C, A'); 166.81 (1C, E'); 177.00 (1C, 1'). ^{31}P NMR (161 MHz, C_6D_6, 343 K) δ ppm: 31.19 (1P, **P**($CHCO_2(CH_2)_2CH_3$)($(CH_2)_3CH_3$)$_3$); 33.36 (1P, **P**($(CH_2)_3CH_3$)$_4$).

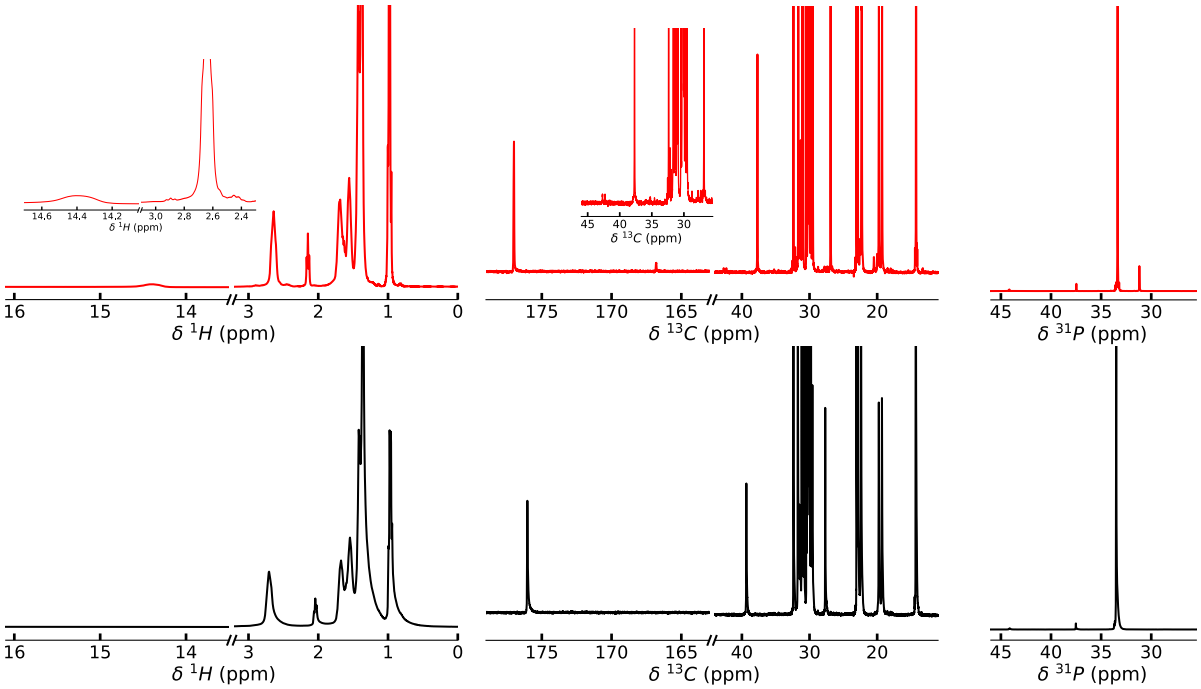

Figure S29 – (Left) ^{1}H, (middle) ^{13}C and (right) ^{31}P NMR spectra of $[P_{6,6,6,14}][C_{11}COO]$ — before and — after CO_2 absorption at 343 K.

4.11 $[P_{4,4,4,4}][Me_4C_4COO]$

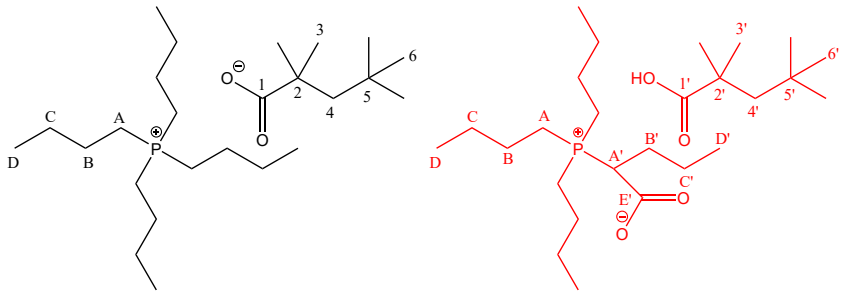

Figure S30 – Chemical structure of the $[P_{4,4,4,4}][Me_4C_4COO]$ (left) before and (right) after CO_2 absorption.

Tetrabutylphosphonium 2,2,4,4-tetramethylpentanoate $[P_{4,4,4,4}][Me_4C_4COO]$ after CO_2 absorption: ^{1}H NMR (400 MHz, C_6D_6, 343 K) δ ppm: 0.93-1.01 (m, 21H, 6 + D + D'); 1.11 (s, 6H, 3'); 1.51 (m, 8H, C + C'); 1.58 (s, 2H, 4'); 1.62 (m, 8H, B + B'); 2.52 (m, 6H, A); 2.69 (m, 8H, A); 2.85 (t, 1H, $^3J_{HH}$

= 12.0 Hz, A'); 17.68 (1H, RCOO**H**). ^{13}C NMR (100 MHz, C_6D_6, 343 K) δ ppm: 13.79 (3C, D); 13.85 (4C, D); 14.20 (1C, D'); 19.24 (4C, A); 19.82 (3C, A); 24.12-24.75 (8C, B + B' + C + C'); 30.05 (2C, 3'); 31.86 (3C, 6'); 32.18 (1C, 5'); 42.61 (1C, A'); 43.13 (1C, 2'); 55.05 (1C, 4'); 166.76 (1C, E'); 180.39 (1C, 1'). ^{31}P NMR (161 MHz, C_6D_6, 343 K) δ ppm: 31.24 (1P, **P**$(CHCO_2(CH_2)_2CH_3)((CH_2)_3CH_3)_3)$; 33.73 (1P, **P**$((CH_2)_3CH_3)_4$).

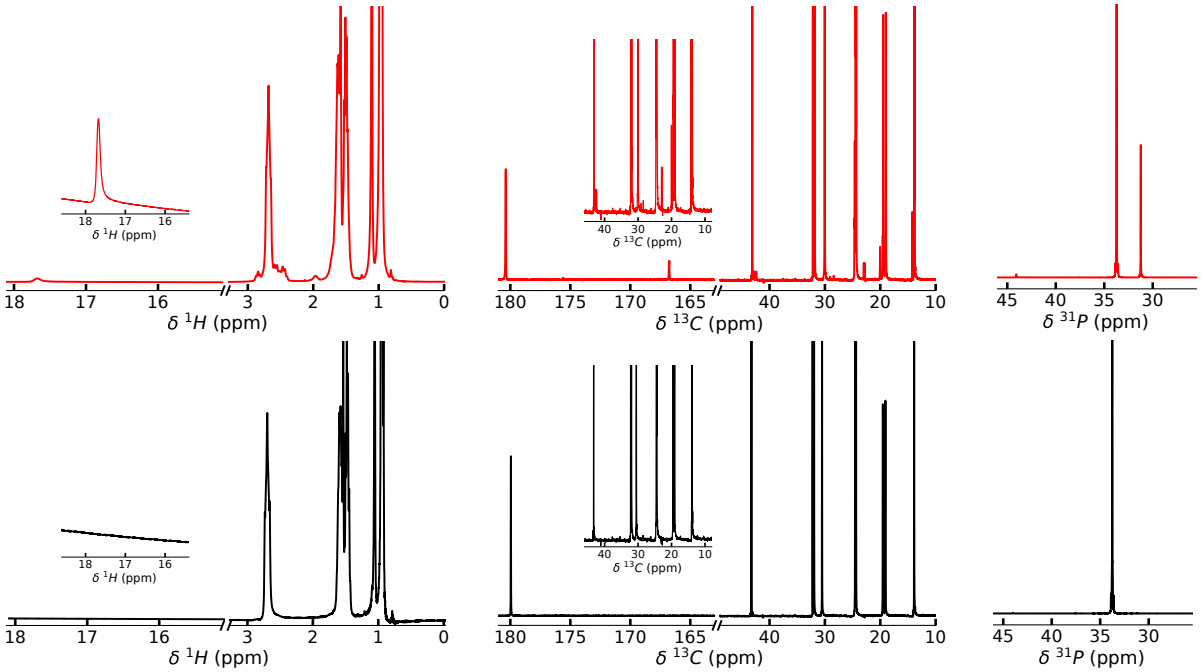

Figure S31 – (Left) ^{1}H, (middle) ^{13}C and (right) ^{31}P NMR spectra of $[P_{4,4,4,4}][Me_4C_4COO]$ — before and — after CO_2 absorption at 343 K.

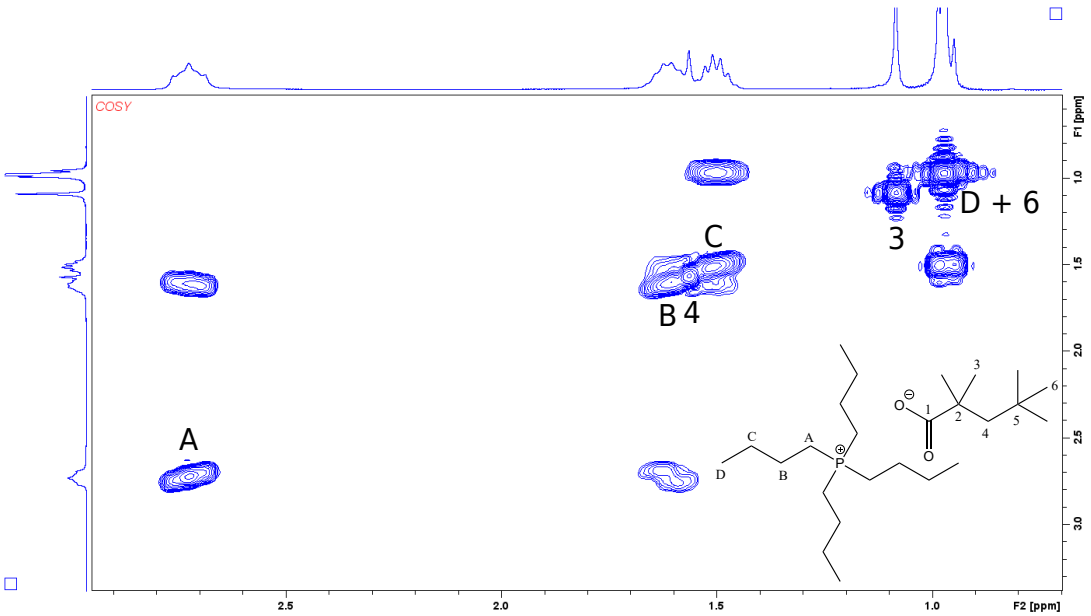

Figure S32 – COSY NMR spectrum of $[P_{4,4,4,4}][Me_4C_4COO]$ at 343 K.

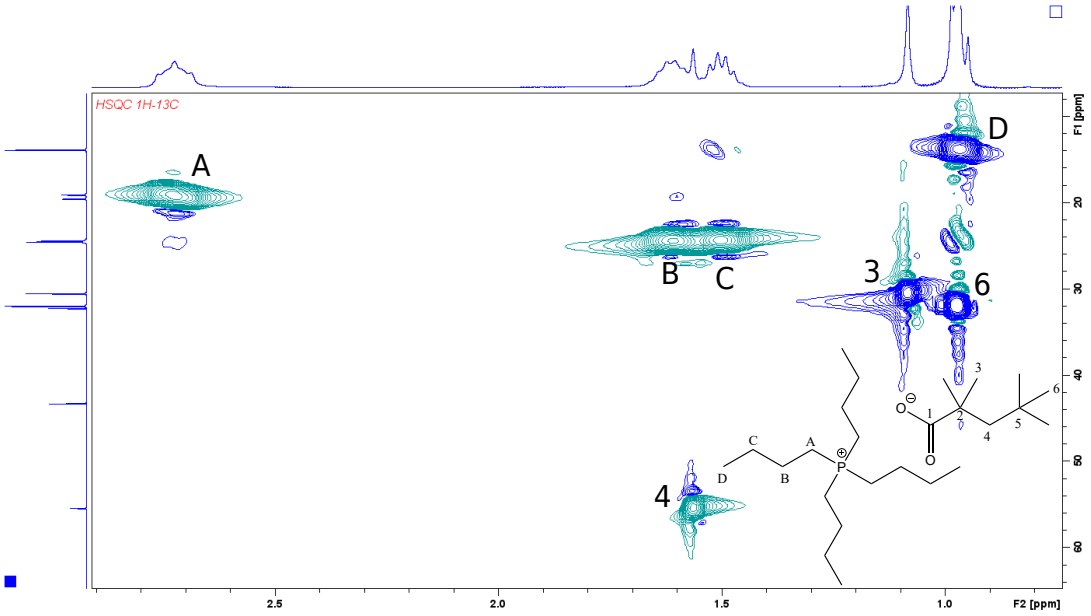

Figure S33 – HSQC NMR spectrum of $[P_{4,4,4,4}][Me_4C_4COO]$ at 343 K.

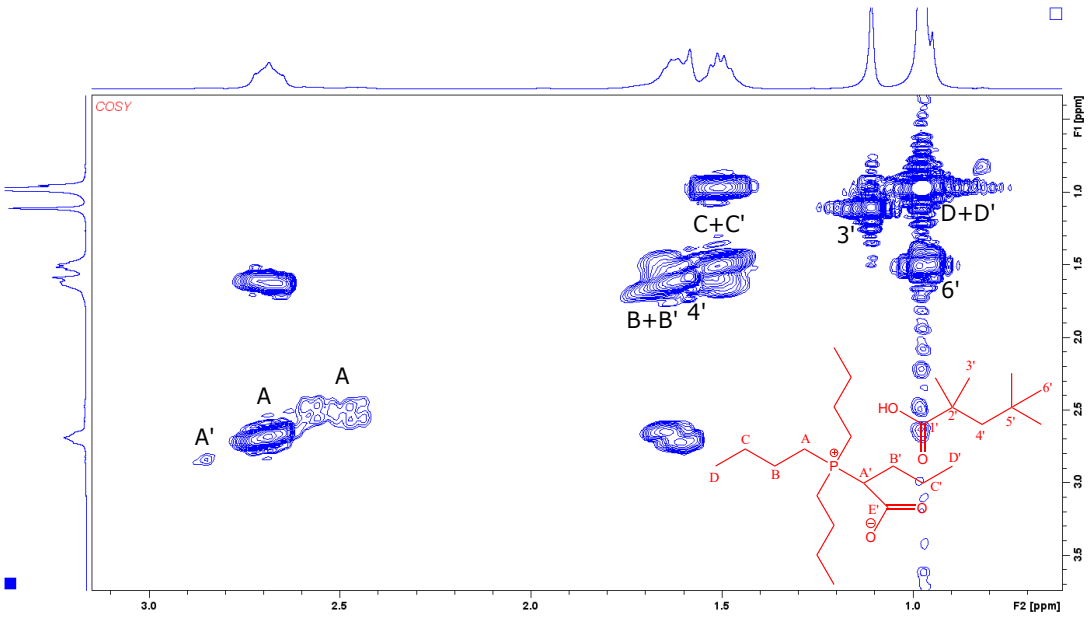

Figure S34 – COSY NMR spectrum of $[P_{4,4,4,4}][Me_4C_4COO]$ after CO_2 absorption at 343 K.

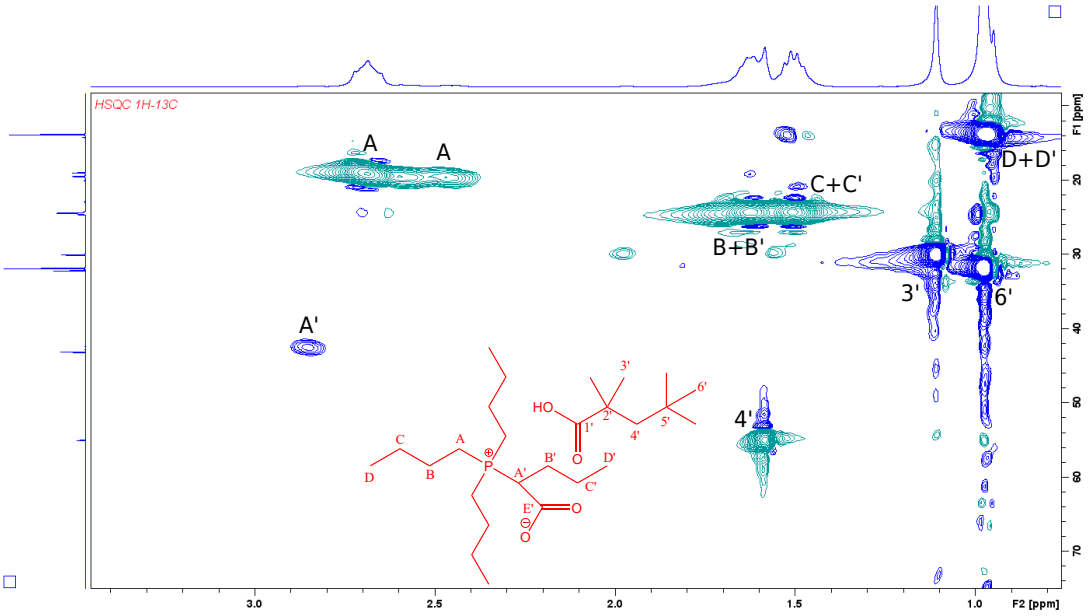

Figure S35 – HSQC NMR spectrum of $[P_{4,4,4,4}][Me_4C_4COO]$ after CO_2 absorption at 343 K.

4.12 $[P_{6,6,6,14}][Me_4C_4COO]$

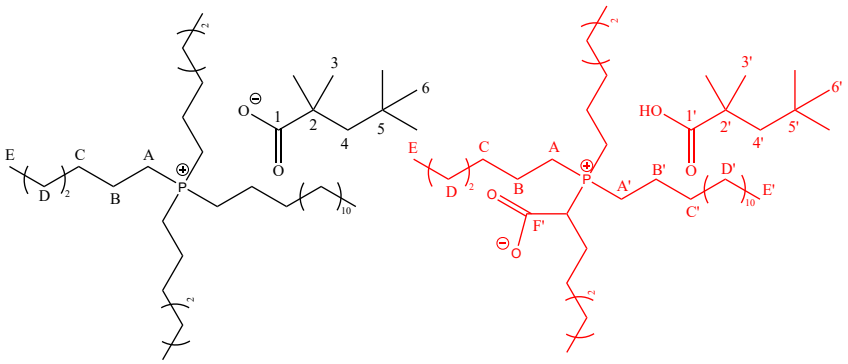

Figure S36 – Chemical structure of the $[P_{6,6,6,14}][Me_4C_4COO]$ (left) before and (right) after CO_2 absorption. For the sack of clarity, the CO_2 absorbed has been represented on one of the hexyl alkyl chain of the phosphonium cation, but it also could be grafted on the tetradecyl alkyl chain without any clear preference.

Trihexyltetradecylphosphonium $[P_{6,6,6,14}][Me_4C_4COO]$ after CO_2 absorption: ^{1}H NMR (400 MHz, C_6D_6, 343 K) δ ppm: 0.89-0.99 (m, 12H, E+E'); 1.02 (s, 9H, 6'); 1.17 (s, 6H, 3'); 1.27-1.46 (m, 32H, D+D'); 1.52 (m, 8H, C + C'); 1.64 (s, 2H, 4'); 1.68 (m, 8H, B+B'); 2.48 (m, 6H, A); 2.73 (m, 8H, A); 2.89 (m, 1H, A'); 17.08 (1H, RCOO**H**). ^{13}C NMR (100 MHz, C_6D_6, 343 K) δ ppm: 14.27, 14.33 (4C, E + E'); 19.55 (4C, A); 20.28 (3C, A); 22.29-22.67 (4C, B+B'); 22.85, 23.02, 29.28-30.25, 31.27-32.53 (25C, D + D'+ 5'); 29.90 (2C, 3'); 30.88-31.25 (4C, C+C'); 31.88 (3C, 6'); 42.42 (1C, A'); 43.06 (1C, 2'); 54.84 (1C, 4'); 166.83 (1C, E'); 180.77 (1C, 1'). ^{31}P NMR (161 MHz, C_6D_6, 343 K) δ ppm: 31.36

(1P, **P**($CHCO_2(CH_2)_2CH_3$)($(CH_2)_3CH_3$)$_3$); 33.64 (1P, **P**($(CH_2)_3CH_3$)$_4$).

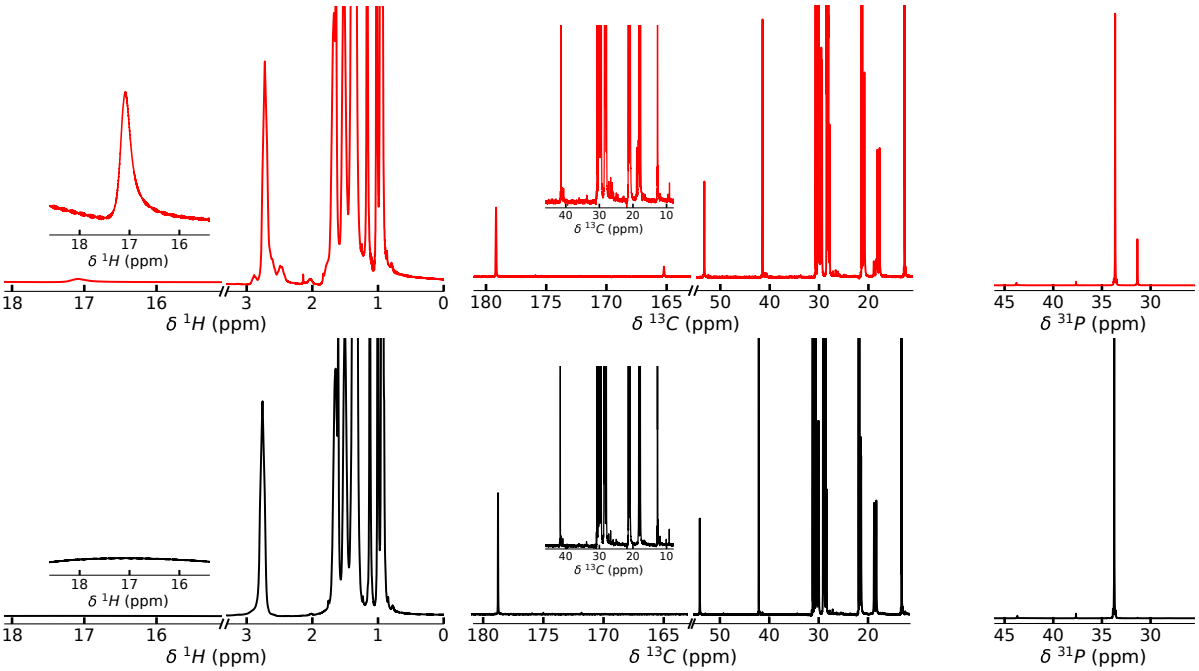

Figure S37 – (Left) ^{1}H, (middle) ^{13}C and (right) ^{31}P NMR spectra of [$P_{6,6,6,14}$][Me_4C_4COO] — before and — after CO_2 absorption at 343 K.

4.13 DOSY experiments

DOSY NMR experiments were conducted on ^{1}H atoms to determine the self-diffusion coefficients (D) of the ions before and after the absorption of CO_2. These measurements aimed to gain insights into the dynamic properties of the ILs. The obtained results are presented in Figure S38, and the exact values can be found in Table S14. As previously emphasized in a relevant study,[1] the self-diffusion coefficients of both the anion and cation in the neat ILs were found to be similar. This observation suggests the presence of strong cation-anion associations, despite the substantial difference in their masses.

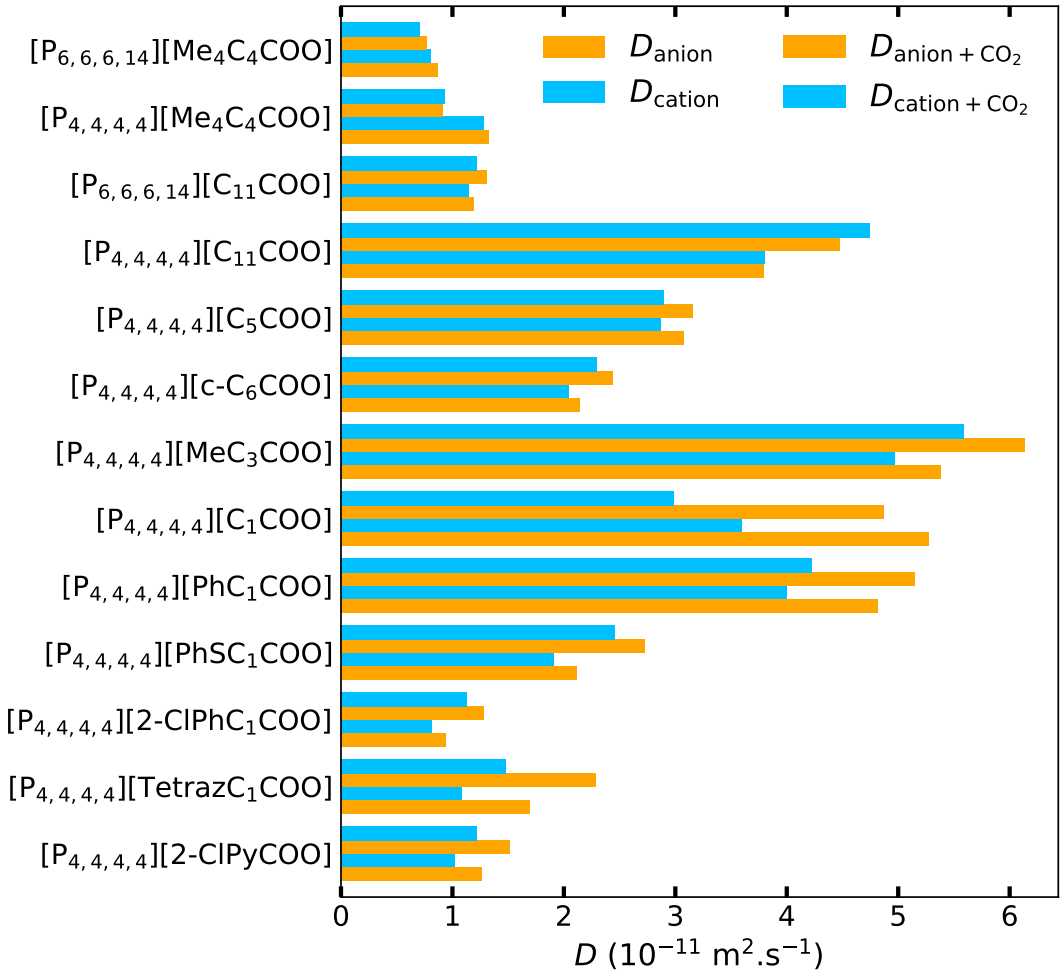

Figure S38 – Histogram representing the experimental self-diffusion coefficients (D) of both the anion and the cation in the ILs before and after being pressurized by CO_2 at 343 K by DOSY-NMR experiments.

Table S14 – Self-diffusion coefficients (D) of the ILs under study at 343 K by DOSY-NMR experiments. The D values of the neat ILs were determined in a previous study.[1]

Sample	$\frac{T}{\mathrm{K}}$	$\frac{D_{\mathrm{anion}}}{10^{-11}\mathrm{m^2\,s^{-1}}}$	$\frac{D_{\mathrm{cation}}}{10^{-11}\mathrm{m^2\,s^{-1}}}$
$[P_{4,4,4,4}][2-ClPyCOO]$	343	1.26 ± 0.04	1.02 ± 0.02
$[P_{4,4,4,4}][2-ClPyCOO] + CO_2$	343	1.51 ± 0.03	1.22 ± 0.02
$[P_{4,4,4,4}][TetrazC_1COO]$	343	1.69 ± 0.008	1.08 ± 0.003
$[P_{4,4,4,4}][TetrazC_1COO] + CO_2$[6]	343	2.28 ± 0.01	1.48 ± 0.009
$[P_{4,4,4,4}][2-ClPhC_1OHCOO]$	343	0.94 ± 0.008	0.81 ± 0.004
$[P_{4,4,4,4}][2-ClPhC_1OHCOO] + CO_2$	343	1.28 ± 0.003	1.13 ± 0.007
$[P_{4,4,4,4}][PhSC_1COO]$	343	2.11 ± 0.007	1.91 ± 0.005
$[P_{4,4,4,4}][PhSC_1COO] + CO_2$	343	2.72 ± 0.005	2.45 ± 0.004
$[P_{4,4,4,4}][PhC_1COO]$	343	4.81 ± 0.01	4.00 ± 0.01
$[P_{4,4,4,4}][PhC_1COO] + CO_2$	343	5.15 ± 0.03	4.22 ± 0.02
$[P_{4,4,4,4}][C_1COO]$	343	5.27 ± 0.01	3.59 ± 0.005
$[P_{4,4,4,4}][C_1COO] + CO_2$	343	4.87 ± 0.02	2.98 ± 0.007
$[P_{4,4,4,4}][MeC_3COO]$	343	5.38 ± 0.02	4.97 ± 0.01
$[P_{4,4,4,4}][MeC_3COO] + CO_2$	343	6.13 ± 0.03	5.59 ± 0.02
$[P_{4,4,4,4}][c-C_6COO]$	343	2.14 ± 0.006	2.04 ± 0.02
$[P_{4,4,4,4}][c-C_6COO] + CO_2$	343	2.44 ± 0.03	2.29 ± 0.01
$[P_{4,4,4,4}][C_5COO]$	343	3.07 ± 0.003	2.87 ± 0.002
$[P_{4,4,4,4}][C_5COO] + CO_2$	343	3.15 ± 0.01	2.89 ± 0.01
$[P_{4,4,4,4}][C_{11}COO]$	343	3.79 ± 0.03	3.80 ± 0.02
$[P_{4,4,4,4}][C_{11}COO] + CO_2$	343	4.47 ± 0.01	4.74 ± 0.02
$[P_{6,6,6,14}][C_{11}COO]$	343	1.19 ± 0.004	1.14 ± 0.004
$[P_{6,6,6,14}][C_{11}COO] + CO_2$	343	1.31 ± 0.003	1.22 ± 0.001
$[P_{4,4,4,4}][Me_4C_4COO]$	343	1.33 ± 0.003	1.28 ± 0.002
$[P_{4,4,4,4}][Me_4C_4COO] + CO_2$	343	0.91 ± 0.002	0.93 ± 0.001
$[P_{6,6,6,14}][Me_4C_4COO]$	343	0.86 ± 0.002	0.80 ± 0.001
$[P_{6,6,6,14}][Me_4C_4COO] + CO_2$	343	0.77 ± 0.002	0.70 ± 0.001

5 FT-IR measurements

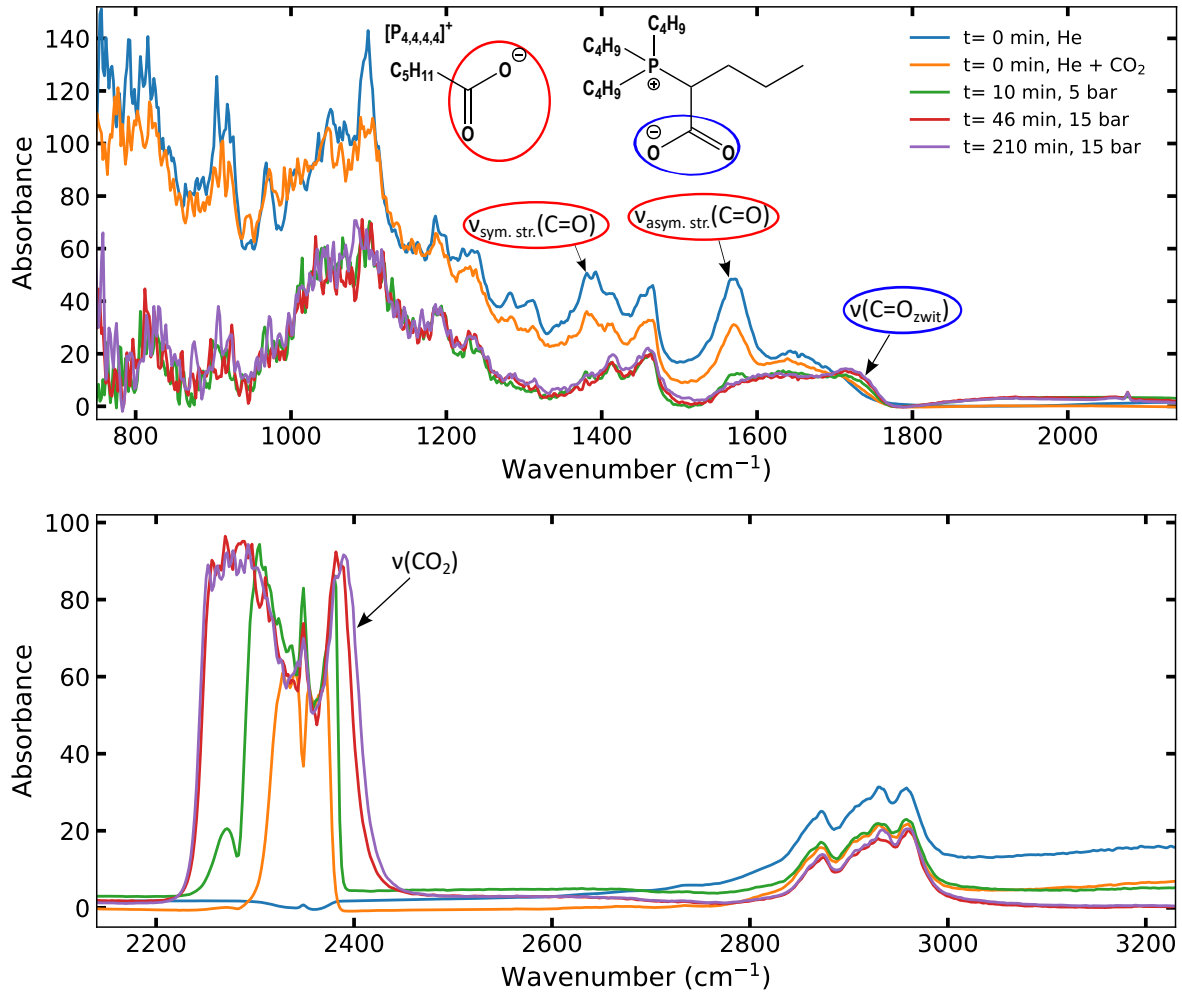

Figure S39 – FT-IR spectrum of $[P_{4,4,4,4}][C_5COO]$ at different time exposure under CO_2 pressure at 303 K from 750 to 3230 cm^{-1}.

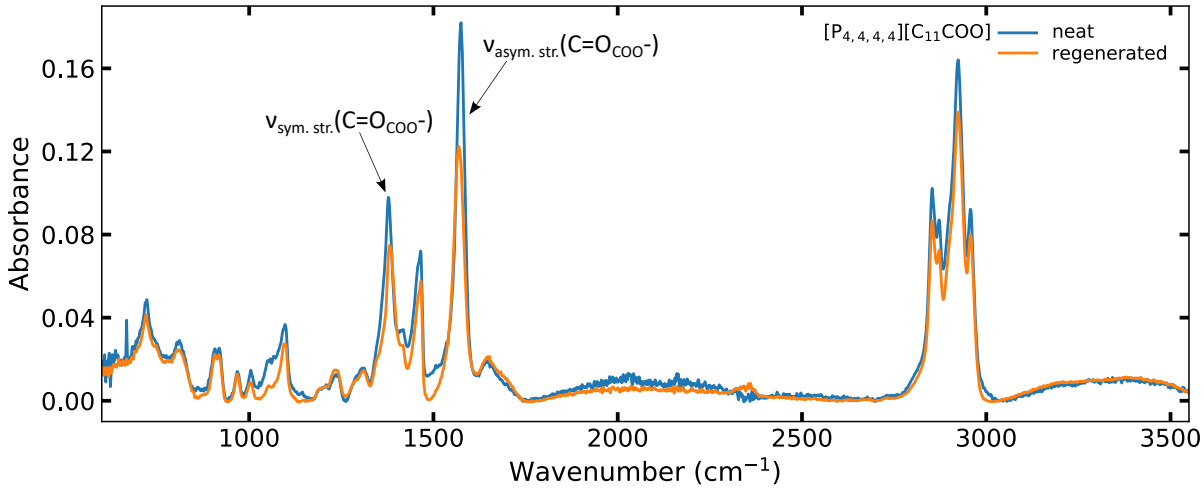

Figure S40 – Comparison of the full FT-IR spectra between the — neat $[P_{4,4,4,4}][C_{11}COO]$ and — post regeneration after 2 cycles of absorption and desorption at 303 K and 343 K.

6 Molecular Dynamics Simulations

MD simulations of the ILs in presence of CO_2 have been carried out as they allow further insights into the molecular structure of the systems to have a better understanding of how CO_2 is solvated. The RDFs of $[P_{4,4,4,4}][C_{11}COO]$ in presence of CO_2, depicted in Figure 8 as representative example of the other ILs, show that there is no modification of the structural organization of the IL induced by the presence of CO_2. Indeed, the distances between the negatively charged O_{COO^-} of the carboxylate anions and the P^+ and the H_α of the phosphonium cation remain the same. The CN of these two different interacting sites remain almost identical to the case without CO_2 as they slightly decrease from 1.01 to 1.00 and 4.53 to 4.51, respectively. The presence of CO_2 into the system does not seem to perturb the interaction between the two ions. The CO_2 molecules are preferentially located around the carboxylate head of the anion with the carbon atoms oriented toward the negatively charged oxygen atoms at 2.183 Å with a coordination number of about 0.04 in $[P_{4,4,4,4}][C_{11}COO]$. More generally, the RDFs and the CNs of these two interacting sites are similar in all the ILs even in the presence of CO_2 (Figure S43). Even the microscopic structures of $[P_{4,4,4,4}][2-ClPyCOO]$ (Figure S44) and $[P_{4,4,4,4}][TetrazC_1COO]$,[6] which were presenting slightly different RDFs because of secondary intermolecular interactions, are not impacted by the presence of CO_2.

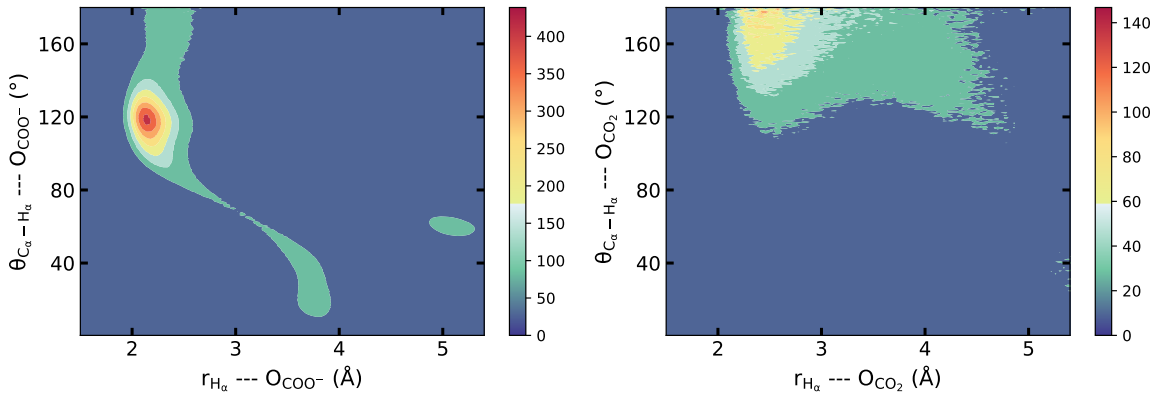

Figure S41 – Combined distribution function of the Angular Distribution Function (ADF) as a function of the RDF in $[P_{4,4,4,4}][C_{11}COO]$ showing the angle between (left) $C_\alpha{-}H_\alpha$ of the $[P_{4,4,4,4}]^+$ cation, (right) the oxygen atoms of CO_2 with the oxygen atoms O_{COO^-} of the carboxylate anion as a function of the distance between the acidic proton H_α and the O_{CO_2} with the negatively charged O_{COO^-} at 343 K, respectively.

The CDFs of the $C_\alpha{-}H_\alpha\cdots O_{COO^-}$ angle as a function of the distance between the acidic proton H_α and O_{COO^-}, and the CDFs of the $C_\alpha{-}H_\alpha\cdots O_{CO_2}$ angle as a function of the distance between the acidic proton H_α and O_{CO_2} in all the ILs under study have been calculated at 343 K, but only the ones of

$[P_{4,4,4,4}][C_{11}COO]$ are depicted Figure S41 for the sack of clarity as they are all similar.

Even in presence of CO_2, the CDFs are similar to the ones of the neat ILs with an $C_\alpha{-}H_\alpha\cdots O_{COO^-}$ angle of approximately 120 ° at a distance about 2.15–2.18 Å at the exception of $[P_{4,4,4,4}][TetrazC_1COO]$ and $[P_{4,4,4,4}][2\text{-}ClPyCOO]$ which exhibit larger angles of about 123.3 °[6] and 124.5 °, respectively. The angles are too low to be considered as proper hydrogen bonds which means that the H_α abstraction is not driven by this interaction. The acid-base equilibrium is not favored by this particular spatial configuration as it is the case with imidazolium carboxylate ILs. Therefore, the differences of absorption capacity are not explained by a particular spatial configuration between the interacting sites revealing that the differences are probably due to thermodynamic features. In imidazolium carboxylate ILs, the proton located on the C_2 position of the 1,3-dialkylimidazolium rings is more acidic. It induces a strong H-bond interaction between O_{COO^-} of the carboxylate and this proton resulting in a more favorable initial deprotonation.[9] It is in line with the higher K_{eq} determined for these imidazolium ILs.[10]

An $C_\alpha{-}H_\alpha\cdots O_{CO_2}$ angle of approximately 179° and a distance of 2.26 Å has been found in all the ILs as illustrated in Figure S41 (right). It indicates the formation of H-bonds between CO_2 and the phosphonium cations, confirming that the most favourable CO_2 solubilization site in phosphonium carboxylate ILs is located between the O_{COO^-} of the anion and the H_α of the cation.

It is interesting to note that in the initial state, the CO_2 molecule is in close proximity to O_{COO^-} and H_α of the phosphonium cation. This observation is consistent with both DFT calculations and MD simulations (Figure S42) indicating that CO_2 is preferentially solvated around the carboxylate head of the anions. This finding suggests that increasing the bulkiness of both the cation and the anion may impede accessibility to the interacting sites, thereby reducing its solubility. This could explain why $[P_{6,6,6,14}][Me_4C_4COO]$ exhibits a lower CO_2 capture capacity compared to its $[P_{4,4,4,4}]^+$ counterparts.

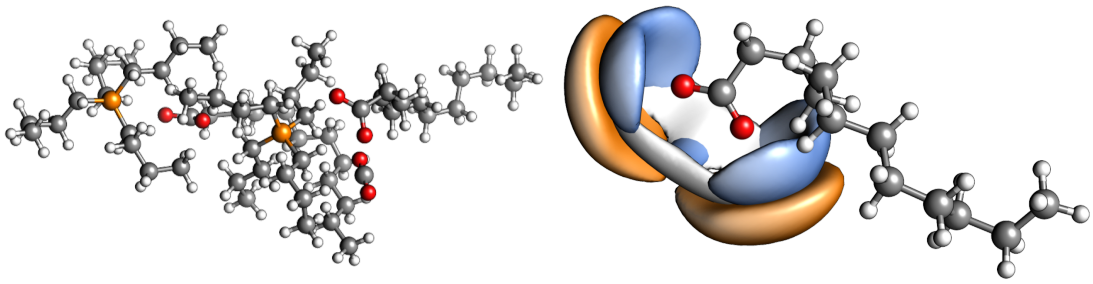

Figure S42 – (Left) The most favorable optimized structure of the initial state in $[P_{4,4,4,4}][C_{11}COO]$ from *ab initio* calculations. (Right) The SDFs of ■ P^+, of □ the acidic protons H_α and of ■ C_{CO_2} around the O_{COO^-} of the $[C_{11}COO]^-$ anion in $[P_{4,4,4,4}][C_{11}COO]$ at 343 K. Isodensity contours at 11.6, 14.1 and 0.8 times the average density around the central anion, respectively.

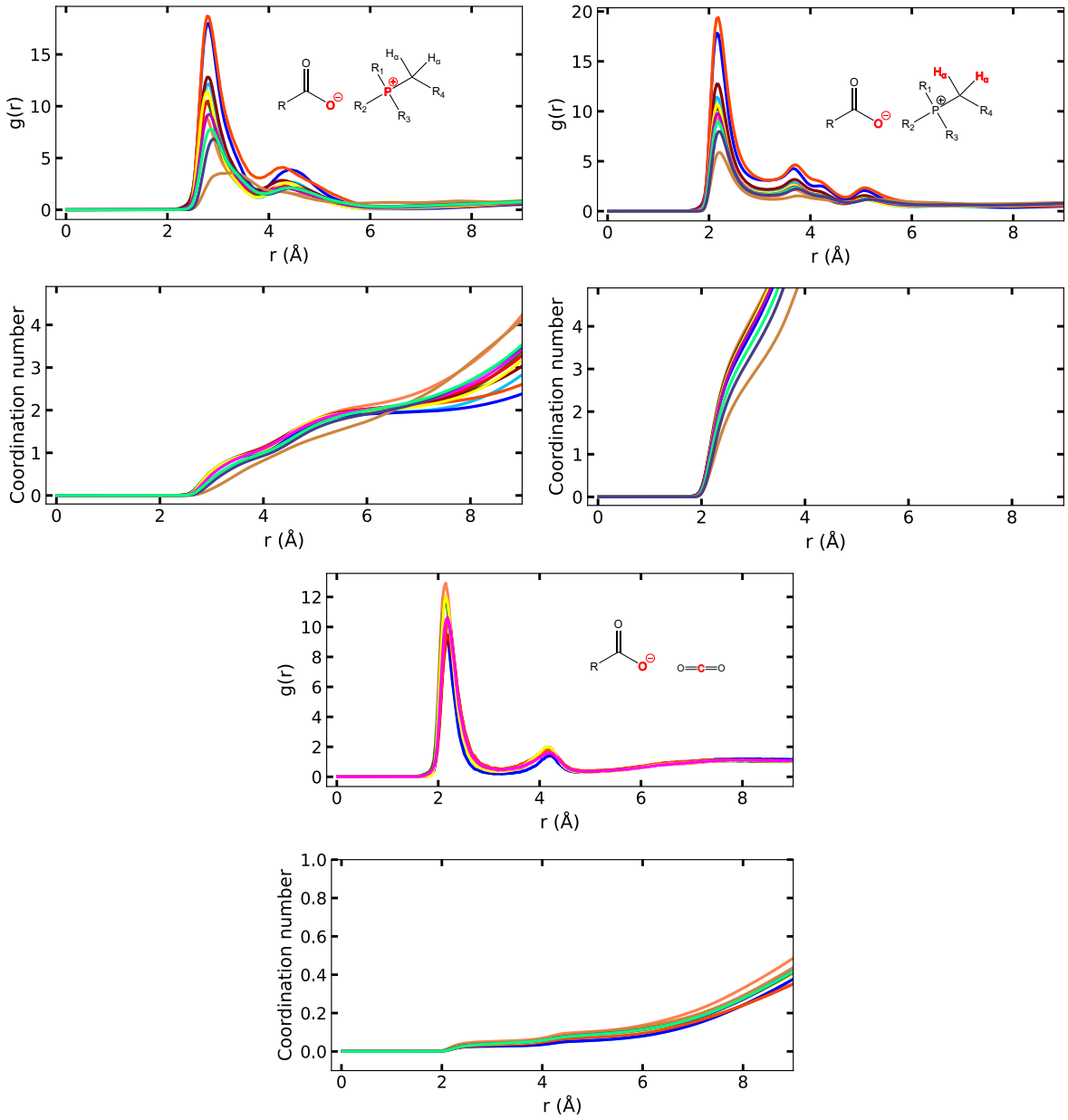

Figure S43 – Comparison of the site-site RDF, $g(r)$, of (top left) P^+ and (top right) H_α of the cation and (bottom) C_{CO_2} of the CO_2 around O_{COO^-} of the carboxylate anion and their corresponding coordination number in carboxylate head of the anion and their corresponding coordination numbers in — $[P_{4,4,4,4}][2-ClPyCOO]$, — $[P_{4,4,4,4}][2-ClPhC_1OHCOO]$, — $[P_{4,4,4,4}][PhSC_1COO]$, — $[P_{4,4,4,4}][PhC_1COO]$, — $[P_{4,4,4,4}][C_1COO]$, — $[P_{4,4,4,4}][MeC_3COO]$, — $[P_{4,4,4,4}][c-C_6COO]$, — $[P_{4,4,4,4}][C_5COO]$, — $[P_{4,4,4,4}][C_{11}COO]$, — $[P_{6,6,6,14}][C_{11}COO]$, — $[P_{4,4,4,4}][Me_4C_4COO]$ and — $[P_{6,6,6,14}][Me_4C_4COO]$ in presence of CO_2 at 343 K.

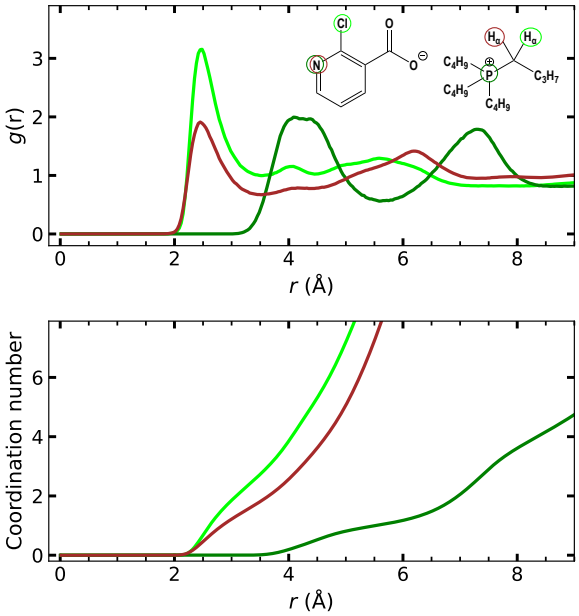

Figure S44 – Site-site RDFs, $g_{ij}(r)$, of H_α around — Cl and — N, — P^+ around N in $[P_{4,4,4,4}][2-ClPyCOO]$ in presence of CO_2 at 343 K.

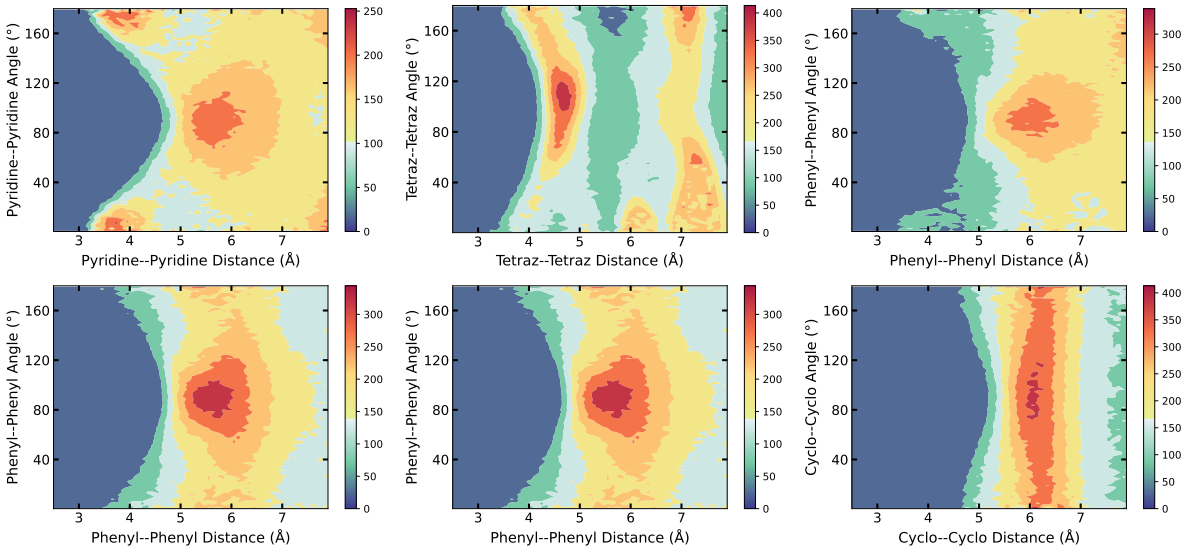

Figure S45 – CDFs of the angle between (top left) two adjacent pyrridine rings in $[P_{4,4,4,4}][2-ClPyCOO]$, (top middle) two adjacent tetrazole rings in $[P_{4,4,4,4}][TetrazC_1COO]$, two adjacent phenyl rings (top right) in $[P_{4,4,4,4}][2-ClPhC_1OHCOO]$, (bottom left) in $[P_{4,4,4,4}][PhSC_1COO]$, (bottom middle) in $[P_{4,4,4,4}][PhC_1COO]$ and (bottom right) two adjacent cyclohexane in $[P_{4,4,4,4}][c-C_6COO]$ as a function of the RDF between their center of mass at 343 K in presence of CO_2.

7 *Ab initio* calculations

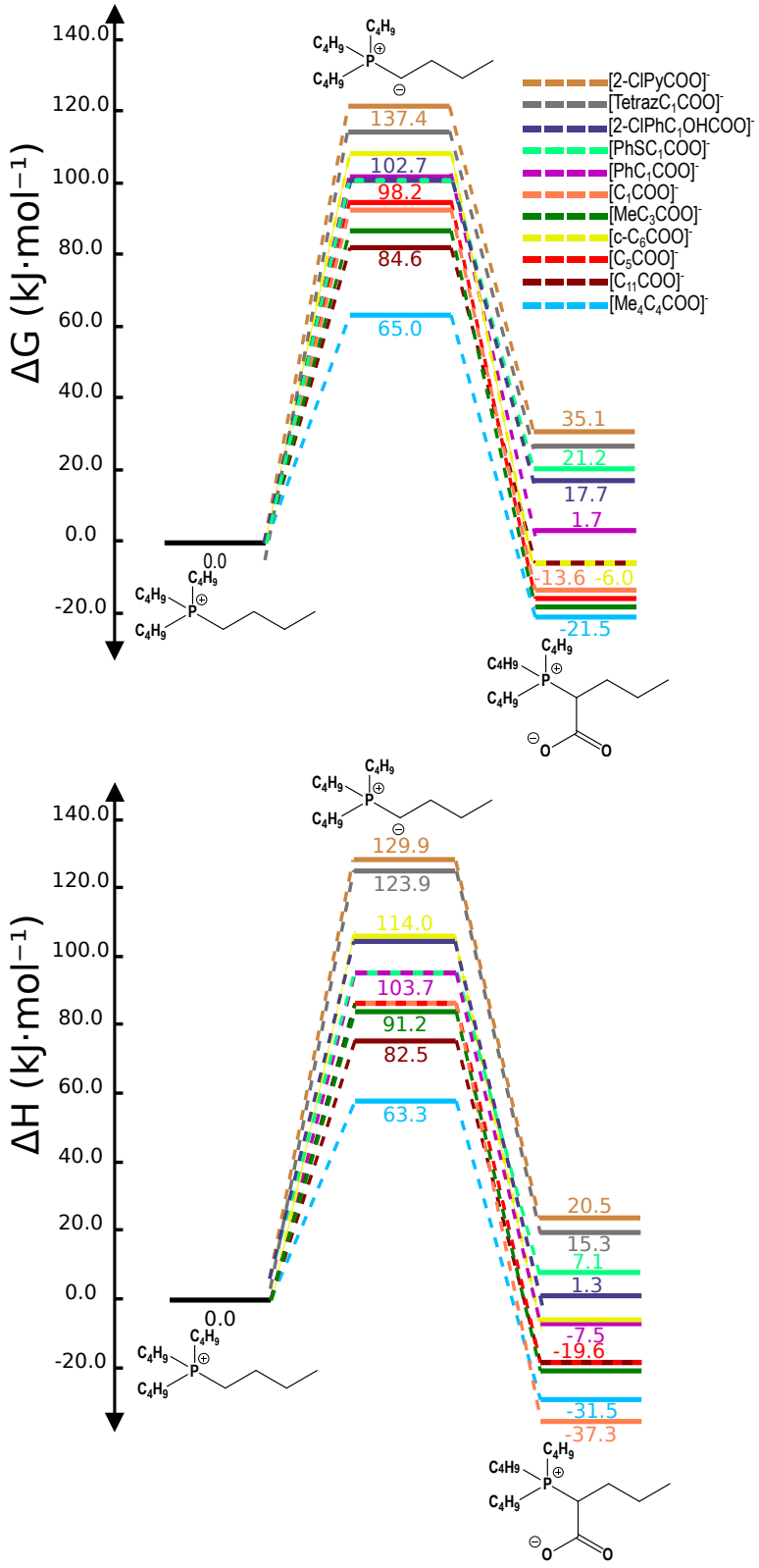

Figure S46 – Relative (top) Gibbs free energy and (bottom) enthalpy of the reactions leading to the chemical capture of CO_2 in — $[P_{4,4,4,4}][2-ClPyCOO]$, — $[P_{4,4,4,4}][TetrazC_1COO]$,[6] — $[P_{4,4,4,4}][2-ClPhC_1OHCOO]$, — $[P_{4,4,4,4}][PhSC_1COO]$, — $[P_{4,4,4,4}][PhC_1COO]$, — $[P_{4,4,4,4}][C_1COO]$, — $[P_{4,4,4,4}][MeC_3COO]$, — $[P_{4,4,4,4}][c-C_6COO]$, — $[P_{4,4,4,4}][C_5COO]$, — $[P_{4,4,4,4}][C_{11}COO]$ and — $[P_{4,4,4,4}][Me_4C_4COO]$ at 343 K with 2:1 stoichiometry (IL:CO_2).

Table S15 – Atomic charges (q) of the different ILs in the initial state (I.S.), intermediate (Interm.) and the final state (F.S.) of the CO_2 absorption mechanism with a 2:1 stoichiometry (IL:CO_2) as well as the related HOMO energy. All the anions are paired with the $[P_{4,4,4,4}]^+$ cation. As the charges carried by the $[P^+_{4,4,4,4}{-}CO_2^-]$ zwitterion and the free CO_2 are approximately 0, they are not displayed for the sack of clarity.

Sample	$q([P_{4,4,4,4}]^+)$	$q([RCOO]^-)$	q(Ylide)	q(RCOOH)	E(HOMO)
	e	e	e	e	eV
[2 −ClPyCOO] I.S.	0.58 & 0.65	-0.60 & -0.63	-	-	-8.02
[2 −ClPyCOO] Interm.	-0.73	-0.52	-0.08	-0.10	-5.57
[2 −ClPyCOO] F.S.	0.57	-0.42	-	-0.08	-7.94
[TetrazC$_1$COO] I.S.[6]	0.78 & 0.53	-0.60 & -0.71	-	-	-6.31
[TetrazC$_1$COO] Interm.[6]	0.72	-0.54	-0.05	-0.11	-4.20
[TetrazC$_1$COO] F.S.[6]	0.73	-0.65	-	-0.11	-6.25
[2 −ClPhC$_1$OHCOO] I.S.	0.71 & 0.58	-0.61 & -0.62	-	-	-7.43
[2 −ClPhC$_1$OHCOO] Interm.	0.61	-0.49	0.00	-0.08	-5.56
[2 −ClPhC$_1$OHCOO] F.S.	0.62	-0.47	-	-0.12	-7.55
[PhSC$_1$COO] I.S.	0.65 & 0.56	-0.58 & -0.62	-	-	-6.84
[PhSC$_1$COO] Interm.	0.52	-0.49	0.09	-0.07	-5.04
[PhSC$_1$COO] F.S.	0.65	-0.54	-	-0.11	-6.94
[PhC$_1$COO] I.S.	0.58 & 0.63	-0.62 & -0.58	-	-	-6.07
[PhC$_1$COO] Interm.	0.70	-0.48	-0.06	-0.17	-4.26
[PhC$_1$COO] F.S	0.57	-0.49	-	-0.10	-6.58
[C$_1$COO] I.S.	0.61 & 0.62	-0.61 & -0.61	-	-	-6.13
[C$_1$COO] Interm.	0.68	-0.51	0.01	-0.16	-4.47
[C$_1$COO] F.S.	0.65	-0.51	-	-0.13	-6.57
[MeC$_3$COO] I.S.	0.62 & 0.65	-0.62 & -0.64	-	-	-6.12
[MeC$_3$COO] Interm.	0.65	-0.54	0.07	-0.17	-4.44
[MeC$_3$COO] F.S.	0.67	-0.52	-	-0.15	-6.52
[c−C$_6$COO] I.S.	0.63 & 0.66	-0.61 & -0.68	-	-	-5.95
[c−C$_6$COO] Interm.	0.76	-0.50	-0.08	-0.15	-4.31
[c−C$_6$COO] F.S.	0.61	-0.49	-	-0.13	-6.53
[C$_5$COO] I.S.	0.63 & 0.62	-0.62 & -0.61	-	-	-6.12
[C$_5$COO] Interm.	0.63	-0.54	0.12	-0.17	-4.72
[C$_5$COO] F.S.	0.71	-0.52	-	-0.13	-6.46
[C$_{11}$COO] I.S.	0.64 & 0.65	-0.62 & -0.64	-	-	-6.02
[C$_{11}$COO] Interm.	0.72	-0.52	-0.01	-0.15	-4.43
[C$_{11}$COO] F.S.	0.64	-0.57	-	-0.11	-6.42
[Me$_4$C$_4$COO] I.S.	0.69 & 0.58	-0.62 & -0.64	-	-	-6.04
[Me$_4$C$_4$COO] Interm.	0.65	-0.57	0.12	-0.17	-4.67
[Me$_4$C$_4$COO] F.S.	0.62	-0.53	-	-0.13	-6.44

In the intermediate state, the formation of the $[P_{4,4,4,4}]$[RCOO]-HOOCR complex is supported by the presence of a slight negative charge on the carboxylic acid between -0.07 and $-0.17e$ with specific values

for each IL reported in Table S15. This charge arises from a transfer of charge from the carboxylate anion to the neutral carboxylic acid, facilitated by the formation of a hydrogen bond. The negative charge carried by $[RCOO]^-$ decreases from approximately $-0.6e$ to $-0.53e$. In the final state, although the partial charge on HOOCR is slightly less negative, the presence of the complex linked by a hydrogen bond is still evident due to a similar charge transfer (between -0.08 and $-0.15e$). The positive charge on the phosphonium cation increases upon the formation of this complex, as the hydrogen bond formation reduces the charge transfer between the cation and the anion.

Molecular orbital analysis was performed on the HOMOs of the CO_2 absorption mechanism steps for each IL, and their corresponding energies are reported in Table S15. This analysis provides insight into the stabilization of ILs upon CO_2 capture. In all cases, the HOMO is destabilized due to the acid-base reaction between the phosphonium cation and the carboxylate anion, as indicated by the positive ΔE. Among the ILs, $[P_{4,4,4,4}][Me_4C_4COO]$ exhibits the smallest ΔE (1.37 eV), which aligns with the most favorable intermediate step discussed earlier. The ΔE values for the other ILs fall within an intermediate range, at the exception of $[P_{4,4,4,4}][TetrazC_1COO]$, $[P_{4,4,4,4}][PhSC_1COO]$, $[P_{4,4,4,4}][2-ClPyCOO]$ and $[P_{4,4,4,4}][2-ClPhC_1OHCOO]$ with higher ΔE. It is in agreement with their highly positive ΔG and the lower basicity of their carboxylate anions. Upon the addition of the ylide to CO_2, a significant stabilization of the HOMOs is observed, leading to a decrease in E(HOMO) by approximately 0.4–0.5 eV compared to the initial state. This decrease indicates that the final state is more energetically favorable compared to the initial state. It aligns with the negative $\Delta_r G°$ values calculated for most ILs, expect for the four previously mentioned ILs, which exhibit almost no reactivity towards CO_2. Only a slightly positive or near-zero variation in E(HOMO) between the final and initial states is noticed which is consistent with the positive $\Delta_r G°$ determined.

The optimized structures of the intermediate step and the final step are shown in Figure S47. In the intermediate state, following the abstraction of the acidic proton by the carboxylate anion, it is possible to observe the newly formed complex between the free pair of IL and the carboxylic acid $[P_{4,4,4,4}][RCOO]$-HOOCR as illustrated in Figure S47 (left). The formation of this complex is driven by the establishment of a hydrogen bond between the negatively charged oxygen atom of the carboxylate and the $-OH$ group of the carboxylic acid. This complex in still present after the addition of the ylide on CO_2 (Figure S47 (right)). In the $[P_{4,4,4,4}][C_{11}COO]$-$HOOCC_{11}$ complex, the distance between the acidic proton and the oxygen atom ($d(OH-OCOO^-)$) is 1.36 Å, while the corresponding angle ($\widehat{OHO}$) is 178.2°, satisfying the hydrogen bond criteria. The values of $d(OH-O_{COO^-})$ and $\widehat{OHO}$ for the other ILs all fall within a similar

range, without any specific correlation between these parameters and the basicity of the carboxylate anion in water.

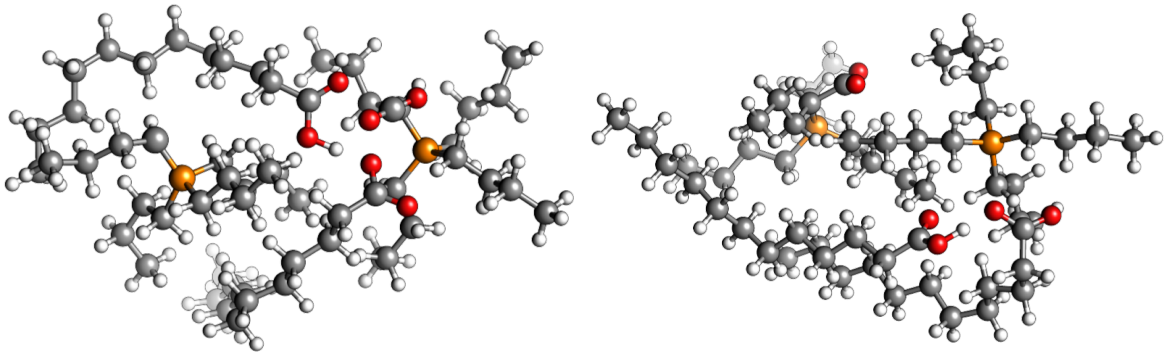

Figure S47 – The most favorable optimized structures of (left) the intermediate state and (right) the product of the reaction between $[P_{4,4,4,4}][C_{11}COO]$ and CO_2 as well as the $[P_{4,4,4,4}][RCOO]$-HOOCR complex.

The peculiar spatial configurations found in the neat ILs containing rings in the carboxylate anions [1] were similar even in presence of CO_2 as depicted on the CDFs of the angle between two adjacent rings as a function of the RDF between their center of mass in the ESI Figure S45.

References

(1) Scaglione, N.; Avila, J.; Bakis, E.; Padua, A.; Gomes, M. C. *Phys. Chem. Chem. Phys.* **2023**, *25*, 15325–15339.

(2) Jacquemin, J.; Ge, R.; Nancarrow, P.; Rooney, D. W.; Costa Gomes, M. F.; Pádua, A. A. H.; Hardacre, C. *J. Chem. Eng. Data* **2008**, *53*, 716–726.

(3) Goodrich, B. F.; de la Fuente, J. C.; Gurkan, B. E.; Lopez, Z. K.; Price, E. A.; Huang, Y.; Brennecke, J. F. *J. Phys. Chem. B* **2011**, *115*, 9140–9150.

(4) Deng, Y.; Morrissey, S.; Gathergood, N.; Delort, A.-M.; Husson, P.; Costa Gomes, M. F. *ChemSusChem* **2010**, *3*, 377–385.

(5) Baranyai, K. J.; Deacon, G. B.; MacFarlane, D. R.; Pringle, J. M.; Scott, J. L. *Aust. J. Chem.* **204**, *57*, 145–147.

(6) Scaglione, N.; Wylie, L.; Padua, A.; Costa Gomes, M. *Submitted* **2024**, *00*, 000–000.

(7) Padua, A. H. Cl&Pol. (accessed 2021); `https://github.com/paduagroup/clandpol`.

(8) Wu, B.; Yamashita, Y.; Endo, T.; Takahashi, K.; Castner, E. W. *J. Chem. Phys.* **2016**, *145*, 244506.

(9) Gurau, G.; Rodríguez, H.; Kelley, S. P.; Janiczek, P.; Kalb, R. S.; Rogers, R. D. Demonstration of Chemisorption of Carbon Dioxide in 1,3-Dialkylimidazolium Acetate Ionic Liquids. *Angew. Chem. Int. Ed.* **2011**, *50*, 12024–12026.

(10) Lepre, L. F.; Szala-Bilnik, J.; Pison, L.; Traïkia, M.; Pádua, A. a. H.; Ando, R. A.; Gomes, M. F. C. Can the tricyanomethanide anion improve CO2 absorption by acetate-based ionic liquids? *Phys. Chem. Chem. Phys.* **2017**, *19*, 12431–12440.